

Ambidexterity and Left-Handedness Induced by Geminally Disubstituted γ Amino Acid Residues in Chiral 3_{10} Helices

Swapna Debnath, Vignesh Shanmugam Rajalakshmi, Dinesh Kumar, Babulal Das, Prema G. Vasudev,* Priyadarshi Satpati,* and Sunanda Chatterjee*



Cite This: *ACS Omega* 2023, 8, 36370–36385



Read Online

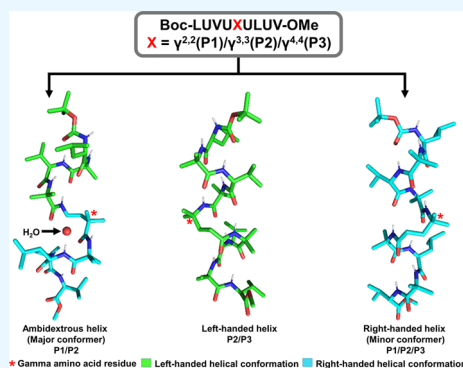
ACCESS |

Metrics & More

Article Recommendations

Supporting Information

ABSTRACT: Chirality is an omnipresent feature in nature's architecture starting from simple molecules like amino acids to complex higher-order structures viz. proteins, DNA, and RNA. The L configuration of proteinogenic amino acids gives rise to right-handed helices. Ambidexterity is as rare in organisms as in molecules. There are only a few reports of ambidexterity in single-peptide molecules composed of either mixed L and D or achiral residues. Here, we report, for the first time, the ambidextrous and left-handed helical conformations in the chiral nonapeptides **P1**–**P3** (Boc-LUVU $\gamma^{x,x}$ ULUV-OMe where U = Aib, $x, x = 2, 2/3, 3/4, 4$), containing chiral L α amino acid residues, in addition to the usually observed right-handed helical conformation. The centrally located achiral γ residue, capable of adopting both left and right-handed helical conformations, induces its handedness on the neighboring chiral and achiral residues, leading to the observation of both left and right-handed helices in **P2** and **P3**. The presence of a single water molecule proximal to the γ residue induces the reversal of helix handedness by forming distinct and stable water-mediated hydrogen bonds. This gives rise to ambidextrous helices as major conformers in **P1** and **P2**. The absence of the observation of ambidexterity in **P3** might be due to the inability of $\gamma^{4,4}$ in the recruitment of a water molecule. Experiments (NMR, X-ray, and CD) and density functional theory (DFT) calculations suggest that the position of geminal disubstitution is crucial for determining the population of the amenable helical conformations (ambidextrous, left and right-handed) in these chiral peptides.



INTRODUCTION

Nature is chiral and manifests this at different levels of complexity. Helices (α , 3_{10} and π) are integral parts of the secondary structural elements of proteins. Naturally occurring helices are right-handed due to the L configuration of the constituent amino acid residues. These have negative signs for both backbone torsion angles (ϕ , ψ) and appear in the bottom left quadrant of the Ramachandran map. However, there are a few examples of short left-handed helices in protein crystal structures composed of all L amino acid residues or a mixture of L and D amino acid residues.^{1,2} Left-handed helices have also been reported in a few small synthetic peptides containing L ω amino acid residues.^{3,4} Ambidexterity is very rarely observed in organisms as well as in molecules. There are only a few examples where blocks of L and D amino acid residues upon being used alternately gave rise to ambidextrous helices both in crystals, solution, and in the gas phase.^{5,6} Gopi and coworkers reported ambidexterity in achiral hybrid $(\alpha\gamma)_n$ peptide molecules, which were composed of achiral α amino acid residue Aib and γ amino acid residue 4-amino-3,3-dimethylbutanoic acid.⁷ Though for achiral peptides, right and left-handed helices are topologically equivalent enantiomers, observation of ambidexterity is still a rare phenomenon. The use of alternating L and D amino acid residues led to the formation of double

helical conformation as in gramicidin or feglymycin, which contained a huge central pore.^{8,9} This structure was stabilized by intermolecular hydrogen bonds between the antiparallel strands of the helix as is present in the β -sheet structures.

Geminally disubstituted α amino acid residues like Aib and Ac₆C and higher homologues of α amino acid residues like β -Ac₆C, Gpn, 4-amino-4,4-dimethylbutanoic acid, etc., have been used in generating helical structures in short synthetic peptides.^{10–25} This is because of the tendency of the flanking torsion angles about the point of disubstitution to adopt gauche conformations, which are well accommodated in the helical structures. Higher homologues of α amino acid residues, called ω amino acid residues, have been accommodated into well-folded helical structures that are stabilized by expanded analogues of the canonical C₁₀/C₁₃ hydrogen bonds that are observed in all α amino acid-containing peptide helices.^{16–35}

Received: July 17, 2023

Accepted: August 29, 2023

Published: September 21, 2023



With the intention of understanding the relative ease of accommodating a single differently geminally disubstituted γ amino acid residue as a guest into all α amino acid-containing peptide helices, without disrupting the helical structure, we have incorporated a single $\gamma^{2,2}$, $\gamma^{3,3}$, or $\gamma^{4,4}$ amino acid residue at the central position of a model chiral α -helical peptide scaffold Boc–Leu–Aib–Val–Aib– $\gamma^{x,x}$ –Aib–Leu–Aib–Val–OMe ($x, x = 2, 2/3, 3/3, 4/4$) to generate peptides **P1**–**P3**, respectively (Figures 1a and S1). The energetics of the experimentally observed conformations of **P1**–**P3** were studied by density functional theory (DFT) calculations.

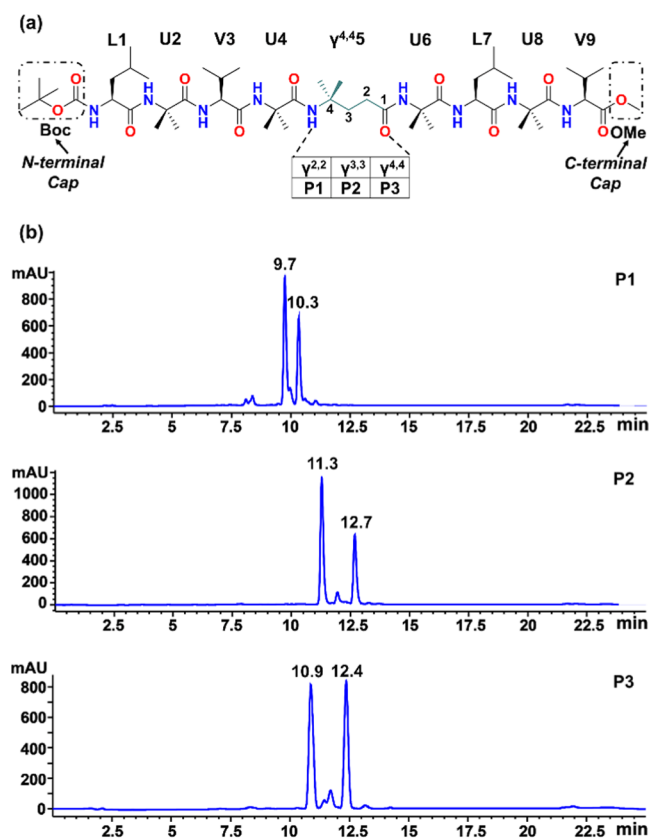


Figure 1. (a) Chemical structure of peptides **P1**–**P3** and (b) analytical HPLC traces of **P1**–**P3** showing the presence of two populants in solution. The populants of **P1**–**P3** are present in the ratios of \sim 60:40, 70:30, and 50:50, respectively.

Herein, we have reported the observation of ambidextrous helix with opposite handedness in single-peptide molecules in crystals and solution of **P1** and **P2**. We have also reported the observation of the left-handed helix (centrally expanded 3_{10} helix) in **P2** and **P3** along with the observation of the usual right-handed helix (centrally expanded 3_{10} helix) in all of the peptides **P1**–**P3**. To the best of our knowledge, this is the first report of an ambidextrous helix and left-handed helices in L amino acid-containing chiral peptides. Hereafter, throughout this study, the “centrally expanded 3_{10} helix” has been abbreviated as the CE 3_{10} helix.

RESULTS AND DISCUSSION

Peptides **P1**–**P3** (Figure 1a) were synthesized using the standard solution-phase synthesis strategy (Scheme S1, Supporting Information (SI)), purified using high-performance liquid chromatography (HPLC), and characterized using

analytical HPLC, matrix-assisted laser desorption/ionization-time of flight (MALDI-TOF), ^1H NMR (600 MHz), and ^{13}C (150 MHz) (Figures S2–S10). It should be noted that all of the ^1H NMR spectra of **P1**–**P3** showed the presence of water peaks (Figures S5–S7), indicating its presence in the solution.

Analytical HPLC. Upon performing analytical HPLC using an ACN/ H_2O solvent system, all of the peptides **P1**–**P3** gave rise to two peaks each in their respective chromatograms (Figure 1b). Table S1 summarizes the retention time of the peaks that appeared in the chromatogram. MALDI-mass spectrometry (MALDI-MS), performed to ascertain the chemical identity of the eluents, indicated an identical molecular mass of the components obtained from the two peaks for all of the peptides (Figures S2–S4 and Table S1). This ruled out the possibility of the presence of impurities and suggested that the peaks were either conformers or diastereomers of **P1**–**P3**. The area under the peaks for the peptides **P1**, **P2**, and **P3** was in the ratios of \sim 6:4, 7:3, and 1:1, respectively. Apart from that, additional small peaks are also observed between the two prominent peaks with identical molecular mass of the peptide, suggesting the presence of other possible conformers in the solution (Figures S11–S13). To understand the retained secondary structure of the two conformers in solution, the isolated fractions were reinjected into the HPLC, and only one peak in the chromatogram for all fractions was observed (Figures S14–S19). For this study, different solvent gradients have been used, due to which the retention time of the individual fractions has changed a bit compared to the previous results shown in Figure 1. However, the difference in the retention time between the two fractions from the same peptide remains intact. Therefore, it is evident that the secondary structures of the conformations are retained in the solution even after the reinjection.

Confirmation of the Presence of Multiple Conformations in Solution for **P1–**P3**.** 1D ^1H NMR. Figure 2 shows the stacked plots of the NH region of 600 MHz ^1H NMR spectra of the peptides **P1**–**P3**. Two prominent sets of peaks were clearly visible in the spectra for all three peptides **P1**–**P3**, in addition to one set of very small peaks, as earlier observed in the analytical HPLC. We have not studied the conformations contributing to the small peaks owing to their very meager population distribution.

Complete annotation of the NMR signals was performed using two-dimensional nuclear magnetic resonance (2D NMR) techniques like total correlation spectroscopy (TOCSY) (Figures S20–S22) and rotating frame Overhauser effect spectroscopy (ROESY). Chemical shifts of all of the signals from the two sets of peaks have been tabulated in the SI (Tables S2–S7). The ratios of the peak intensities for the two sets of peaks were 6:4, 7:3, and \sim 1:1 for **P1**, **P2**, and **P3**, respectively, which were similar to the ratios of the area under the peaks obtained in analytical HPLC earlier. This suggested that the purified peptides were a mixture of two distinct species in solution, which could either be diastereomers or conformers. Both sets of peaks in the spectra were completely well-dispersed for each peptide **P1**–**P3**, which indicated a well-folded structure for the peptides.

Variable Temperature NMR. In order to determine the effect of temperature on the population of the species observed for **P1**–**P3** in solution, we performed variable temperature NMR experiments. Upon heating/cooling, the rate of interconversion of the conformers becomes faster/slower, thereby altering the appearance of the signals.³⁶ Figures 3, S23

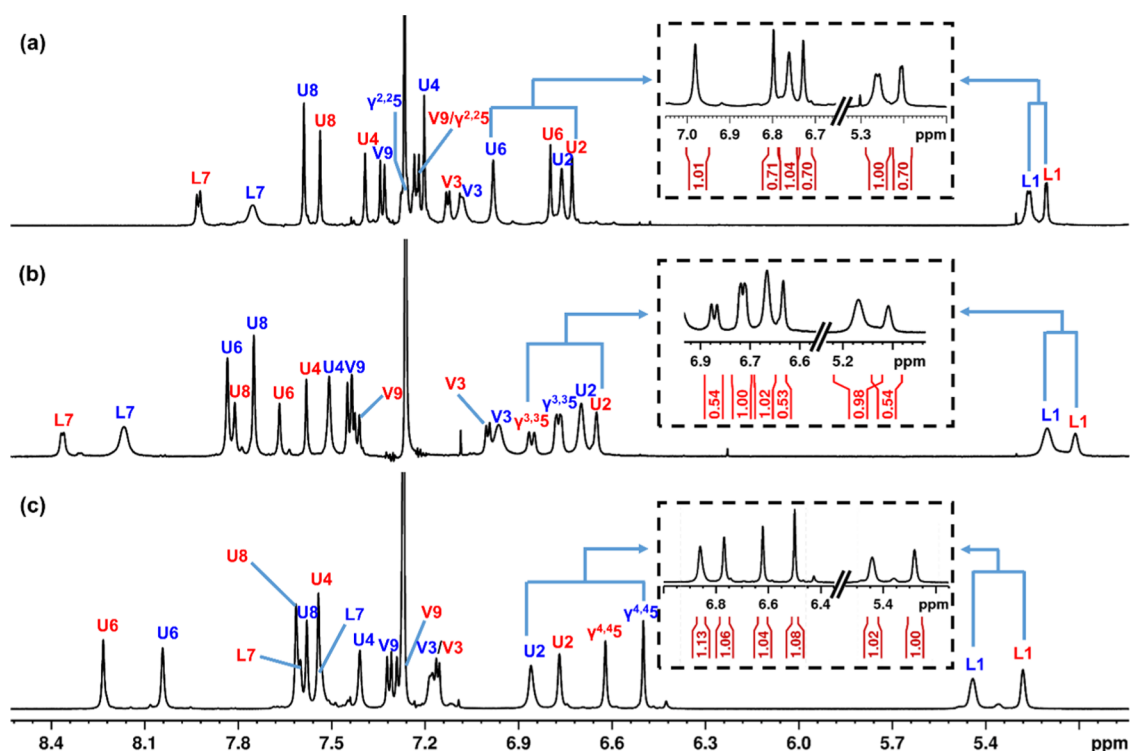


Figure 2. Partial 1D ^1H NMR spectra representing the amide proton resonances of (a) **P1**, (b) **P2**, and (c) **P3** in CDCl_3 at 298 K. Two distinct sets of peaks (labeled in red and blue) are present in all three peptides. The integration of the NH signals corresponding to the ratio of the two populants is highlighted in the dotted box. The intensities for the two sets of peaks for **P1**–**P3** are in the ratio of $\sim 60:40$, $70:30$, and $50:50$, respectively.

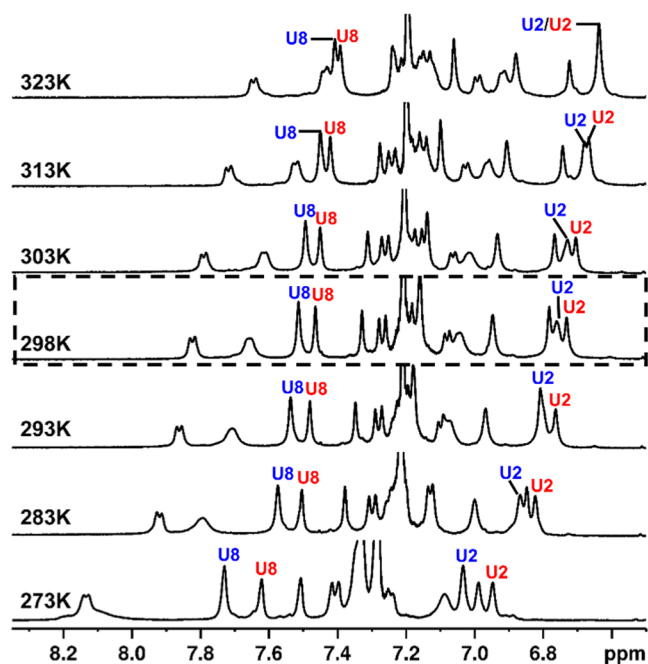


Figure 3. Temperature dependence of NH resonances of **P1** in CDCl_3 . The NH signals marked as blue and red approach closer/ eventually merge with increasing temperature.

and S24 show the NH region of the ^1H NMR spectra recorded at variable temperatures in the range of 273–323 K for **P1** and **P2/P3**, respectively. For all three peptides, both the chemical shifts of the signals and the appearance of the spectral lines changed upon varying the temperature. There was a general

upfield shift of the NH resonances, owing to the breakdown in the hydrogen bonds, upon increasing the temperature, suggesting a well-formed secondary structure of the peptides in solution. Interestingly, a few of the NMR peaks from the same protons in the two populants came closer and finally merged at higher temperatures. In **P1** (Figure 3), a clear merging of the Aib (2) and Aib (8) NH resonances was seen upon increasing the temperature. In the case of **P3**, some of the peaks came closer [set of $\gamma^{4,4}$ (5) peaks], broadened [set of Aib (2) peaks], and eventually coalesced [set of Val (3) peaks] (Figure S24, marked protons) upon increasing the temperature. Such a change in the peak widths and coalescing of the NH signals of two different populants suggested that the populants must be in exchange with each other. Observation of two sets of peaks at room temperature indicated that the rate of interconversion between the different conformers was slow at room temperature in the NMR timescale. This slow interconversion, in turn, indicated that the conformations were separated by a large activation barrier in the energy landscape. Hence, it might be concluded from the above experiment that each of the peptides **P1**–**P3** existed as two distinct conformers at room temperature, as reported earlier in related studies.³⁷ The populations of the two conformers of **P1**, **P2**, and **P3** were 60:40, 70:30, and 53:47, respectively (Figure 2) in solution. As everything else in **P1**–**P3** was identical except the constituent γ amino acid residue in question, the differential population of the conformers of **P1**–**P3** in solution seemed to be controlled by the variable position of the backbone disubstitution in the γ amino acid residues.

Molecular Conformations of P1–P3 in Crystals. The molecular conformation of the nonapeptides **P1**–**P3** is shown in Figure 4. The values of the backbone torsion angles are

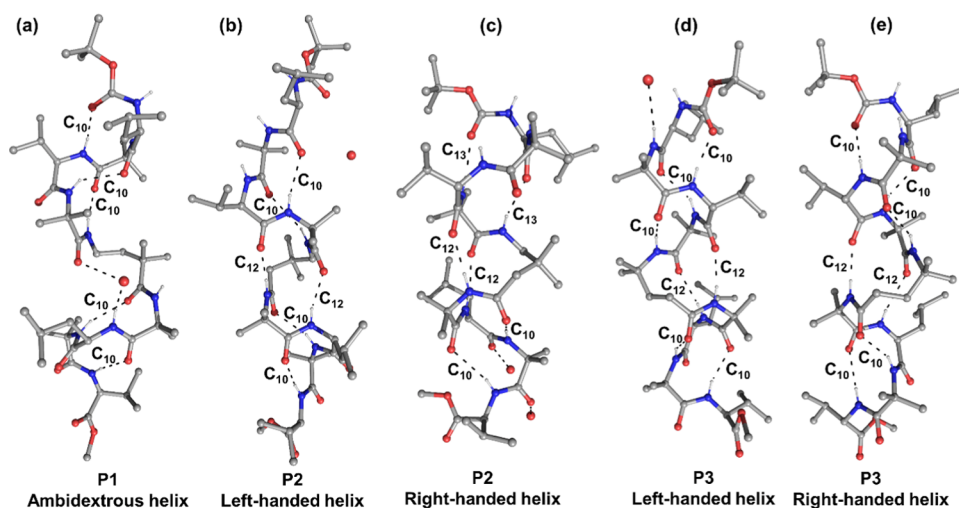


Figure 4. Conformations in crystals of (a) **P1** (CCDC No. 2206582), (b, c) **P2** (2206583, 2206584), and (d, e) **P3** (2206585, 2206586). (a) **P1** forms an ambidextrous helix with left-handedness in the N-terminal (Res 1–4) and right-handedness at the C-terminal (Res 5–9). A centrally recruited water molecule (red sphere) mediated intramolecular hydrogen bond involving Leu (7) NH and Aib (4) CO induces the reversal of handedness. It is stabilized by C_{10} hydrogen bonds. **P2** forms both (b) left-handed CE $_{3,10}$ helix and (c) right-handed CE $_{3,10}$ helix. **P3** also forms both (d) left-handed and (e) right-handed CE $_{3,10}$ helices. The water molecules shown in (b), (c), and (d) do not participate in intramolecular hydrogen bonds.

listed in Table 1 and the hydrogen bond parameters are listed in Table 2. Peptides **P2** and **P3** generated polymorphic crystals depending on the process of crystallization, which had different conformations.

All of the peptides adopted helical conformations. The backbone conformation of γ amino acid residues is defined by four torsion angles, ϕ ($C\alpha'-N1-C\gamma-C\beta$), θ_1 ($N1-C\gamma-C\beta-C\alpha$), θ_2 ($C\gamma-C\beta-C\alpha-C'$), and ψ ($C\beta-C\alpha-C'-N2$). The dimethyl substitution at the $C\alpha$, $C\beta$, and $C\gamma$ atoms promoted *gauche* conformation about the flanking single bonds in the $\alpha/\beta/\gamma$ -disubstituted γ amino acid residues ($\gamma^{2,2}$, $\gamma^{3,3}$, $\gamma^{4,4}$), as evidenced by Table 1. The remaining two dihedral angles showed torsion angle values close to 90 or 180°.

P1 crystals were obtained from a mixture of the two conformers in the ACN/H $_2$ O solvent system. **P1** adopted an ambidextrous helical conformation, stabilized by five 10-atom hydrogen bonds (C_{10}) (Figure 4a). A reversal of the handedness of the helix was observed in the middle of the helix, near the $\gamma^{2,2}$ residue. Inspection of the ϕ and ψ values in Table 1 showed that amino acid residues 1–4 and 5–9 adopted positive and negative values of ϕ/ψ , respectively, suggesting that **P1** adopted left-handedness at the N-terminus and right-handedness at the C-terminus. The $\gamma^{2,2}$ amino acid residue showed a folded conformation with both ϕ and ψ adopting negative values (right-handed helical conformation), while θ_1 and θ_2 corresponded to *gauche+* (*g+*) conformation. The combination of signs of the torsion angles of $\gamma^{2,2}$ was similar to that previously reported for the C_9 and C_{12} helical turns in Gpn/ $\gamma^{3,3}$ amino acid-containing peptides.^{7,24} However, the $\gamma^{2,2}$ amino acid residue formed neither C_9 nor C_{12} hydrogen bonds in **P1**. The reversal of handedness in the peptide helix was induced by the insertion of a water molecule near the $\gamma^{2,2}$ residue that formed hydrogen bonds to Aib (4) CO and Leu (7) NH, which otherwise might have formed a $\gamma\alpha$ C_{12} hydrogen bond. It is worth mentioning that this is the first report of the accommodation of $\gamma^{2,2}$ amino acid residues in an overall helical conformation. Aib (6) NH forms an intermolecular hydrogen bond to Val (3) CO of a neighboring molecule in the crystal lattice (Table 2).

P2, containing $\gamma^{3,3}$, showed three different conformations in its polymorphic crystals. (a) **P2** crystallized from the mixture of the two conformers in ACN/MeOH/H $_2$ O led to orthorhombic crystals, wherein it adopted a left-handed helical conformation, with reversal of handedness of the terminal amino acid residues [Leu (1) and Val (9)], as compared to the rest of the helix (Figure 4b). The peptide was stabilized by six two residue hydrogen bonds: four C_{10} hydrogen bonds (two each at N- and C-termini) and two C_{12} hydrogen bonds in the center (Figure 4b). The first hydrogen bond between the Val (3) NH and Boc (0) CO was obliterated by the N-terminal reversal in handedness. (b) The monoclinic **P2** polymorph grown from the minor peak isolated from the preparative HPLC in ACN/H $_2$ O adopted a right-handed CE $_{3,10}$ helix. It was stabilized by six intramolecular N–H...O hydrogen bonds: two C_{13} 's at the N-terminus, two central $\alpha\gamma/\gamma\alpha$ C_{12} 's, and two C_{10} 's at the C-terminus (Figure 4). The combination of ϕ , θ_1 , θ_2 , and ψ for the $\gamma^{3,3}$ -amino acid residue was $-++-$, with θ_1 and θ_2 adopting *g+* conformations. Both ϕ and ψ adopted values around $\sim-120^\circ$, which was earlier reported for C_{12} helical conformations of $\gamma^{3,3}$ /Gpn.^{7,24} (Table 1). However, no reversal of handedness is observed in this case. (c) **P2** was also crystallized from the mixture of two conformers in ACN/H $_2$ O. However, due to weak X-ray diffraction from this crystal, a well-refined structure could not be obtained. Preliminary structure calculation from this data showed that **P2**, in this case, adopted an ambidextrous helical (Figure S25) structure similar to that observed for **P1** (Figure 4) with small differences as follows (i) the $\gamma^{3,3}$ amino acid residue adopted a left-handed helical conformation in **P2** unlike the right-handed conformation adopted by the $\gamma^{2,2}$ residue in **P1**. (ii) An isolated one residue C_9 hydrogen bond was formed in between Aib (4) CO and Aib (6) NH across the central $\gamma^{3,3}$ amino acid residue, unlike **P1**. The combination of the signs of torsion angles of the $\gamma^{3,3}$ amino acid residue was $(+--+)$, which was exactly the opposite (being left-handed helical) to that observed for Gpn in the right-handed C_9 helical conformation.²⁴

Table 1. Backbone Dihedral Angles of Various Conformations for Peptides P1–P3 Obtained in Crystals and from DFT Calculations (in Parentheses)^a

peptide	amino acid residue	Φ (°)	θ_1 (°)	θ_2 (°)	ψ (°)
P1 (AH)	Leu (1)	66.8 (67.3)			27.1 (25.7)
	Aib (2)	49.3 (55.1)			37.9 (29.7)
	Val (3)	54.6 (61.2)			39.6 (25.1)
	Aib (4)	69.6 (59.7)			4.8 (24.4)
	$\gamma^{2,2}$ (5)	-117.2 (-125.9)	75.0 (93.0)	61.5 (72.0)	-166.6 (-135.5)
	Aib (6)	-58.3 (-56.1)			-36.9 (-39.2)
	Leu (7)	-61.4 (-70.8)			-26.1 (-5.0)
	Aib (8)	-59.9 (-58.0)			-31.8 (-27.7)
	Val (9)	-78.2 (-117.4)			170.4 (163.9)
P1 (RHH)	Leu (1)	(-73.2)			(-19.7)
	Aib (2)	(-55.0)			(-28.2)
	Val (3)	(-60.5)			(-26.7)
	Aib (4)	(-58.0)			(-27.9)
	$\gamma^{2,2}$ (5)	(-84.0)	(161.3)	(-62.1)	(-54.6)
	Aib (6)	(-56.3)			(-37.7)
	Leu (7)	(-61.0)			(-22.1)
	Aib (8)	(-66.9)			(-23.3)
	Val (9)	(-103.3)			(2.2)
P2 (AH)	Leu (1)	60.7 (68.1)			27.8 (22.0)
	Aib (2)	50.8 (54.4)			27.1 (29.8)
	Val (3)	67.3 (68.0)			10.7 (9.0)
	Aib (4)	53.0 (52.6)			29.4 (40.9)
	$\gamma^{3,3}$ (5)	99.3 (107.3)	-64.1 (-59.3)	-79.3 (-81.5)	85.0 (75.9)
	Aib (6)	-56.1 (-54.1)			-35.6 (-35.6)
	Leu (7)	-66.9 (-76.2)			-11.8 (-3.9)
	Aib (8)	-54.4 (-66.7)			-35.3 (-24.8)
	Val (9)	-127.2 (-105.4)			15.4 (-1.7)
P2 (LHH)	Leu (1)	-74.4 (-105.7)			-34.6 (-0.9)
	Aib (2)	58.3 (61.5)			41.7 (28.0)
	Val (3)	62.7 (72.0)			14.4 (6.4)
	Aib (4)	52.2 (56.7)			40.8 (34.9)
	$\gamma^{3,3}$ (5)	135.5 (125.1)	-57.4 (-54.3)	-54.6 (-58.0)	112.7 (124.6)
	Aib (6)	53.2 (57.7)			40.6 (33.9)
	Leu (7)	63.2 (59.4)			11.1 (19.8)
	Aib (8)	46.9 (60.0)			39.9 (26.9)
	Val (9)	-57.8 (-69.5)			-38.7 (-24.2)
P2 (RHH)	Leu (1)	-59.8 (-66.0)			-38.6 (-33.4)
	Aib (2)	-51.2 (-57.8)			-37.8 (-31.9)
	Val (3)	-92.3 (-93.3)			-46.0 (-42.4)
	Aib (4)	-57.1 (-57.8)			-37.4 (-39.1)
	$\gamma^{3,3}$ (5)	-124.8 (-121.3)	55.0 (54.4)	56.5 (59.2)	-117.0 (-123.9)
	Aib (6)	-51.2 (-56.8)			-43.7 (-35.3)
	Leu (7)	-74.9 (-73.4)			-7.5 (-3.4)
	Aib (8)	-59.7 (-63.9)			-31.8 (-27.1)
	Val9	-127.2 (-106.8)			-14.8 (0.0)
P3 (LHH)	Leu (1)	63.9 (66.7)			19.3 (27.0)
	Aib (2)	48.9 (55.1)			35.0 (28.4)
	Val (3)	60.9 (62.9)			29.3 (21.9)
	Aib (4)	56.4 (56.3)			38.0 (34.8)
	$\gamma^{4,4}$ (5)	55.4 (52.4)	53.0 (51.9)	-142.0 (-138.5)	110.1 (115.3)
	Aib (6)	51.1 (56.8)			33.2 (30.3)
	Leu (7)	56.6 (58.0)			32.0 (24.3)
	Aib (8)	68.9 (62.7)			11.1 (25.7)
	Val (9)	-84.5 (-101.3)			-51.1 (-44.5)
P3 (RHH)	Leu (1)	-62.8 (-72.9)			-20.7 (-20.3)
	Aib (2)	-48.6 (-54.7)			-34.7 (-28.4)
	Val (3)	-61.9 (-62.5)			-27.0 (-23.6)
	Aib (4)	-54.5 (-57.5)			-39.7 (-34.3)
	$\gamma^{4,4}$ (5)	-54.7 (-54.4)	-51.6 (-54.3)	142.8 (143.5)	-103.6 (-109.8)
	Aib (6)	-53.8 (-57.0)			-34.7 (-32.4)

Table 1. continued

peptide	amino acid residue	Φ ($^{\circ}$)	θ_1 ($^{\circ}$)	θ_2 ($^{\circ}$)	ψ ($^{\circ}$)
	Leu (7)	-65.6 (-70.9)			-16.9 (-8.8)
	Aib (8)	-62.3 (-63.8)			-22.2 (-22.5)
	Val (9)	-58.2 (-93.7)			133.7 (-50.2)

^aAH: Ambidextrous helix, LHH: left-handed helix, and RHH: right-handed helix.

P3 adopted both left and right-handed CE₃₁₀ helical conformations stabilized by a continuous stretch of two residue backbone N–H···O hydrogen bonds in two different crystals. (a) In the crystal grown from the mixture of two conformers in ACN/H₂O, the peptide formed a left-handed helix, as evidenced by the sign of backbone torsion angles listed in Table 1. In this case, the C-terminal L-Val (9) residue showed a reversal in handedness and adopted a right-handed helical conformation (Figure 4d). Leu (1) at the N-terminus remained in a left-handed helical conformation due to an intermolecular hydrogen bond between Leu (1) NH of one molecule to the Aib (8) CO of another molecule (Table 2). The structure was stabilized by seven intramolecular hydrogen bonds: Five C₁₀ hydrogen bonds (N- and C-termini) and two central C₁₂ hydrogen bonds across the $\alpha\gamma/\gamma\alpha$ segments. (b) In the other crystal for **P3**, grown from the later eluting HPLC fraction (retention time 12.4 min), the peptide adopted a right-handed CE₃₁₀ helical conformation with no reversal of handedness at the helix termini. This structure was also stabilized by a total of seven hydrogen bonds, five C₁₀'s and two C₁₂'s. The backbone dihedral angles of the $\gamma^{4,4}$ amino acid residue adopted a usual (+–+) and (––+) combination in the left and right-handed C₁₂ helical conformations, respectively, as was earlier reported by Gopi and coworkers.²⁵ Both the structures obtained for **P3** were enantiomeric to each other (in the middle stretch), except at the C-terminal Val (9) residue.

Solution Conformational Studies. Infrared Spectroscopy. Figure S26 demonstrates the stacked plots of solution Fourier transform infrared (FTIR) spectroscopy for **P1–P3** in CDCl₃ (1 mM) at room temperature. The characteristic peak at ~ 1650 cm⁻¹ in the spectra of all of the peptides **P1–P3** indicated that all of them adopted a helical conformation.^{38,39}

NMR Spectroscopy. The chemical shift index for the peptides **P1–P3** was calculated by comparing the C ^{α} H chemical shifts observed in CDCl₃ with the random coil shifts obtained from the Bio Mag Res Bank (BMRB)⁴⁰ and the original report of Wishart, Sykes, and Richards⁴¹ (Figure S27). Upfield shifts in the C ^{α} H resonances (negative chemical shift index) of the residues 1, 3, and 7 in both the conformers of **P1**, **P2**, and **P3** indicated helical conformations in them. It should be noted here that the positive chemical shift index observed for the C-terminal residue Val (9) might have resulted in local deviation in the secondary structure due to C-terminal fraying.

The helical conformation of **P1–P3** was further confirmed by low values (~ 5 – 7 Hz) of ³J_{NH–C ^{α} H} coupling constants for all chiral L amino acid residues [Leu (1), Val (3), Leu (7), Val (9)] (Tables S2–S7).

ROESY

In an attempt to further understand the secondary structure of the two conformations of **P1–P3** in detail, we performed the ROESY experiment. Figures Sa–b and S28 represent the partial NH–C ^{α} H/C ^{α} H and NH–NH regions, respectively, of the ROESY spectrum of **P1**. Most of the sequential d_{NN} NOEs

were present for both the conformers. However, both in the major and the minor conformers, the 5/6 d_{NN} NOE was not observed. The NOEs observed for both the conformers were more or less similar with some exceptions. For example, NOEs $\gamma^{2,2}$ (5) C ^{γ} H \leftrightarrow Leu (7) NH and $\gamma^{2,2}$ (5) C ^{γ} H \leftrightarrow Aib (8) NH were weak and medium for the major conformer, while they were both strong in intensity for the minor conformer. Leu (1) C ^{α} H \leftrightarrow Aib (2) NH NOE was stronger and Leu (7) C ^{α} H \leftrightarrow Leu (7) NH NOE was weaker in intensity for the major conformer with respect to the minor. A careful examination of the interproton distances in the conformation of **P1** obtained from crystals (Figure 4a) and comparison with the intensities of the observed NOEs matched it to the major conformation obtained in solution (Figure 5). A large interproton distance of 5.6 Å between the $\gamma^{2,2}$ (5) NH and Aib (6) NH in the major conformer (Figure 5c) explained the absence of the NOE in between them. Thus, the major conformer of **P1** present in solution was the ambidextrous helix, while the minor conformer was still unknown. In the case of **P2** (Figure S29), all of the sequential d_{NN} NOEs were present in both conformers. However, the intensity of the 5/6 d_{NN} NOE across the $\gamma^{3,3}$ residue was weaker compared to all of the other sequential d_{NN} NOEs across the α amino acid residues (Figure S29b). This could be explained by the shorter interproton d_{NN} distances across the α residues (~ 2.4 – 2.8 Å) in contrast to longer interproton d_{NN} distances across the γ residues (~ 3.6 – 4.2 Å) in the helical conformations obtained in crystals (Figures 4c and S29d). Alternating strong and weak NOEs across α and γ amino acid residues in the helical conformation of $\alpha\gamma$ peptides have been reported earlier in the literature.²⁴ Moreover, long-range NOEs like 2/4 d_{NN} NOE and 1/4 C ^{α} H \leftrightarrow NH NOE were observed for the minor conformer, while 7/9 long-range C ^{α} H \leftrightarrow NH NOE was observed for both of them (Figure S29a,b). These observations accompanied by stronger intraresidue C ^{α} H_(i) \leftrightarrow NH_(i) NOEs over inter-residue C ^{α} H_(i) \leftrightarrow NH_(i+1) NOE intensities, suggested that both the conformers were helical. Careful analysis of the differences in the NOE intensities of the two conformers correlated to the interproton distances observed in the conformations obtained in crystals confirmed that the major and the minor conformers for **P2** in solution were the ambidextrous helix and the right-handed CE₃₁₀ helix, respectively (Figure S29). A crucial NOE that helped in the identification of the conformers was the 5/7 C ^{γ} H \leftrightarrow NH NOE, which was present in the minor conformer (interproton distance of 2.7 Å) and absent for the major conformer (interproton distance of 5.0 Å). In the case of **P3**, all of the characteristic NOE features (presence of sequential d_{NN} NOEs, weaker d_{NN} NOE intensities across the $\gamma^{4,4}$ residue in comparison to the α residues, stronger intraresidue C ^{α} H \leftrightarrow NH NOEs) complying with the helical conformation were observed (Figure S30). The NOEs for both the conformers were identical and matched well with the CE₃₁₀ helical conformation observed in crystals (Figure S30). Thus, it can be concluded that the two conformers for **P3** were the left and right-handed CE₃₁₀ helices. The observation of two distinct

Table 2. Intramolecular and Intermolecular Hydrogen Bond Parameters from Various Conformations of P1–P3 Obtained in Crystals and DFT Studies (Mentioned in Parentheses)^a

peptide	H-bonded ring size	H-bonds	D...A (Å)	H...A (Å)	∠ D–H...A (°)		
P1 (AH)	intermolecular	N1–H1...O7 ^a	2.85	1.98	170.3		
		N2–H2...O8 ^a	3.24	2.51	140.3		
		N6–H6...O3 ^b	3.12	2.29	157.4		
		N7–H7...O1W	2.92 (3.0)	2.14 (2.0)	148.3 (167.3)		
		O6...O1W	3.23				
		intramolecular	O4...O1W	(2.7)	(1.7)	(177.1)	
	C ₁₀		N3–H3...O0	3.03 (3.3)	2.21 (2.3)	155.7 (173.1)	
	C ₁₀		N4–H4...O1	3.03 (3.2)	2.31 (2.2)	138.6 (168.0)	
	C ₁₀		N5–H5...O2	3.01 (3.1)	2.16 (2.1)	162.1 (162.6)	
	C ₁₀		N8–H8...O5	3.21 (3.2)	2.38 (2.2)	157.1 (165.7)	
P1 (RHH)	C ₁₀	N9–H9...O6	3.24 (3.2)	2.36 (2.2)	173.3 (167.4)		
		N3–H3...O0	(3.4)	(2.4)	(172.8)		
		N4–H4...O1	(3.1)	(2.1)	(167.2)		
		N5–H5...O2	(3.1)	(2.1)	(163.9)		
		N7–H7...O4	(2.9)	(2.0)	(159.3)		
		N8–H8...O5	(3.3)	(2.3)	(166.7)		
P2 (AH)	C ₁₀	N9–H9...O6	(3.3)	(2.3)	(170.1)		
		N3–H3...O0	2.94 (3.4)	1.96 (2.4)	173.9 (177.8)		
		N4–H4...O1	2.92 (3.1)	1.96 (2.1)	164.6 (169.8)		
		N5–H5...O2	2.98 (3.3)	2.02 (2.3)	164.5 (165.1)		
		O3...O1W	4.05 (3.0)	4.11 (2.1)	79.7 (150.9)		
		O4...O1W	2.96 (3.0)	2.61 (2.1)	101.2 (154.2)		
		N7...O1W	2.99 (3.1)	2.03 (2.1)	165.0 (166.9)		
		N6–H6...O4	2.82 (3.0)	1.85 (2.0)	169.8 (171.9)		
		N8–H8...O5	2.87 (3.2)	1.92 (2.2)	161.7 (166.2)		
		N9–H9...O6	3.22 (3.5)	2.28 (2.5)	157.6 (168.2)		
P2 (LHH)	intermolecular	N1–H1...O7 ^c	3.14	2.31	164.2		
		N2–H2...O8 ^c	3.03	2.19	167.4		
	intramolecular	C ₁₀	N4–H4...O1	3.13 (3.1)	2.28 (2.1)	168.9 (168.0)	
		C ₁₀	N5–H5...O2	3.43 (3.7)	2.60 (2.7)	163.3 (167.1)	
		C ₁₂	N6–H6...O3	2.88 (3.1)	2.02 (2.1)	173.0 (169.1)	
		C ₁₂	N7–H7...O4	2.94 (3.0)	2.12 (2.0)	158.4 (159.5)	
		C ₁₀	N8–H8...O5	2.99 (3.2)	2.16 (2.2)	160.7 (169.3)	
		C ₁₀	N9–H9...O6	3.09 (3.2)	2.25 (2.2)	165.1 (173.4)	
		P2 (RHH)	intermolecular	N1–H1...O2W ^d	3.24	2.37	169.6
				N2–H2...O1W ^d	2.97	2.21	144.5
	N3–H3...O0			3.16 (3.18)	2.45 (2.23)	139.0 (156.8)	
	C ₁₃			N4–H4...O0	2.94 (3.3)	2.07 (2.3)	171.6 (170.8)
	P3 (LHH)	intramolecular	C ₁₃	N5–H5...O1	3.00 (3.3)	2.14 (2.3)	162.4 (164.7)
			C ₁₂	N6–H6...O3	2.92 (3.1)	2.04 (2.1)	173.6 (171.0)
C ₁₂			N7–H7...O4	2.90 (3.0)	2.05 (2.1)	162.0 (166.8)	
C ₁₀			N8–H8...O5	3.05 (3.1)	2.21 (2.2)	159.9 (166.8)	
C ₁₀			N9–H9...O6	3.35 (3.4)	2.49 (2.4)	166.4 (169.1)	
P3 (LHH)			intermolecular	N1–H1...O8 ^e	2.82	1.97	160.9
				N2–H2...O1w	3.28	2.40	171.9
			intramolecular	C ₁₀	N3–H3...O0	2.95 (3.3)	2.09 (2.3)
	C ₁₀	N4–H4...O1		2.93 (3.1)	2.14 (2.1)	149.3 (168.1)	
	C ₁₀	N5–H5...O2		3.15 (3.3)	2.39 (2.3)	145.5 (162.8)	
	C ₁₂	N6–H6...O3		2.87 (3.1)	2.01 (2.0)	165.6 (171.9)	
	C ₁₂	N7–H7...O4		2.97 (3.2)	2.16 (2.2)	152.5 (156.3)	
	C ₁₀	N8–H8...O5		3.01 (3.2)	2.21 (2.2)	150.5 (168.6)	
	C ₁₀	N9–H9...O6		2.96 (3.2)	2.10 (2.2)	163.8 (167.6)	

Table 2. continued

peptide	H-bonded ring size	H-bonds	D...A (Å)	H...A (Å)	∠ D-H...A (°)	
P3 (RHH)	intermolecular	N1-H1...O8 ^f	2.86	2.00	172.5	
		N2-H2...O9 ^f	3.08	2.31	148.6	
	intramolecular	C ₁₀	N3-H3...O0	3.05 (3.4)	2.21 (2.4)	164.8 (172.4)
		C ₁₀	N4-H4...O1	2.90 (3.1)	2.11 (2.1)	151.8 (167.3)
		C ₁₀	N5-H5...O2	3.19 (3.3)	2.43 (2.4)	147.2 (162.3)
		C ₁₂	N6-H6...O3	2.91 (3.0)	2.05 (2.0)	170.9 (173.6)
		C ₁₂	N7-H7...O4	3.19 (3.6)	2.35 (2.7)	164.2 (163.8)
		C ₁₀	N8-H8...O5	3.00 (3.1)	2.19 (2.2)	155.9 (167.6)
		C ₁₀	N9-H9...O6	3.11 (3.3)	2.27 (2.3)	164.2 (165.4)

^aAH: Ambidextrous helix, LHH: left-handed helix, and RHH: right-handed helix.

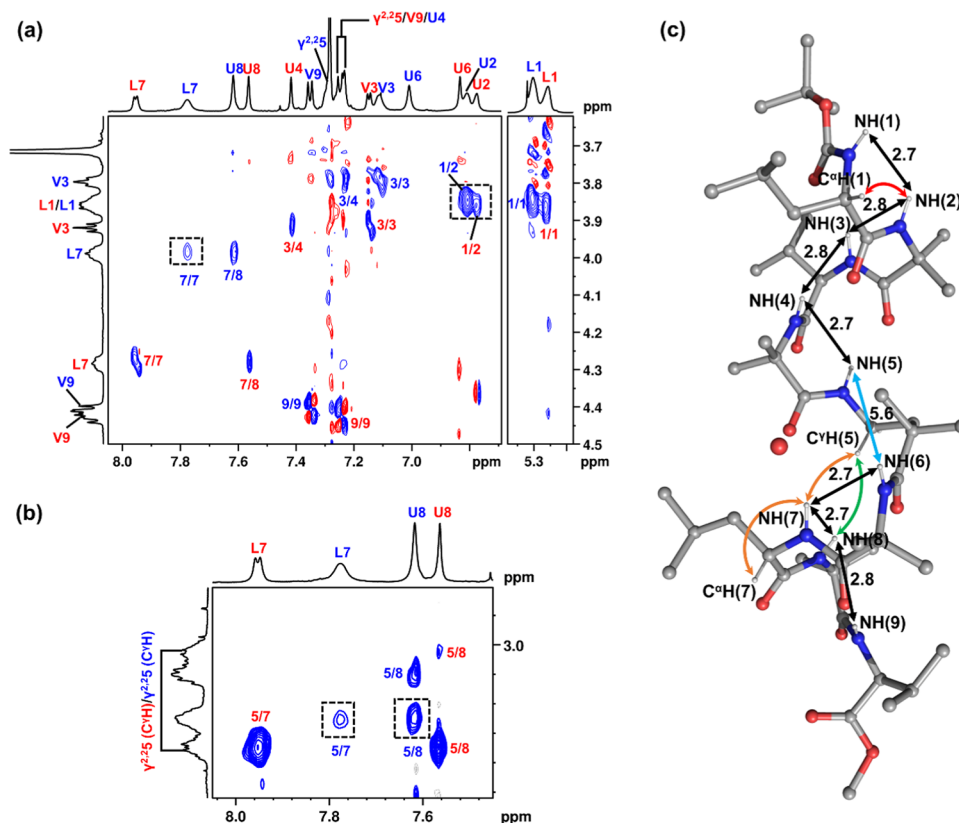


Figure 5. Partial 600 MHz ROESY spectra of **P1** representing (a) NOEs between NH ↔ C^αH and (b) NH ↔ C^βH (γ^{2,2} residue) protons in CDCl₃ at 298 K. (c) Crystal structure of ambidextrous helical **P1** showing the notable NOEs [red (strong), green (medium) and orange (weak) arrows] observed for the major conformer in solution. The d_{NN} distance across the α residues and the γ^{2,2} (5)-Aib (6) segment are shown by black and cyan blue arrows, respectively.

sets of peaks (with nearly equal intensities) in NMR for these two almost enantiomeric (in the middle stretch of the helix) helices might be justified by a minor deviation in the conformation at the helix termini (Val (9) residue), giving rise to diastereomeric helices.

DMSO-*d*₆ Titration. To further confirm the secondary structures of the conformers of **P1–P3** from their hydrogen bonding pattern, DMSO-*d*₆ solvent titration was performed and its results were compared with the crystal structures. Upon addition of polar DMSO-*d*₆ to solution of peptides in nonpolar CDCl₃, solvent-accessible nonhydrogen-bonded NHs form H-bonds with DMSO-*d*₆ and move downfield. The intramolecularly H-bonded NHs on the other hand are solvent inaccessible and do not move. Figures 6, S31 and Table S8

show the change in the chemical shift values of the NH resonances of the conformers of **P1–P3** upon addition of 40% DMSO-*d*₆ to their CDCl₃ solution (~5–7 mM). In **P1**, both the major and the minor conformers have completely solvent-exposed Leu (1) and Aib (2) NH's (Δδ > 1.3 ppm) and partially solvent-exposed Aib (6) NH (Δδ ~ 0.6 ppm) (Figure 6a). Earlier, from the NOE studies, the **P1** major conformer was determined to be an ambidextrous helix as observed in the crystals (Figure 4a). In the crystal structure, all of Leu (1), Aib (2) and Aib (6) NH's were nonhydrogen-bonded intramolecularly and hence expected to be solvent-exposed, showing similar shifts (Δδ ppm) in the DMSO-*d*₆ titration. The lesser shift for Aib (6) observed could be attributed to its crowded hydrophobic environment, limiting the approach of

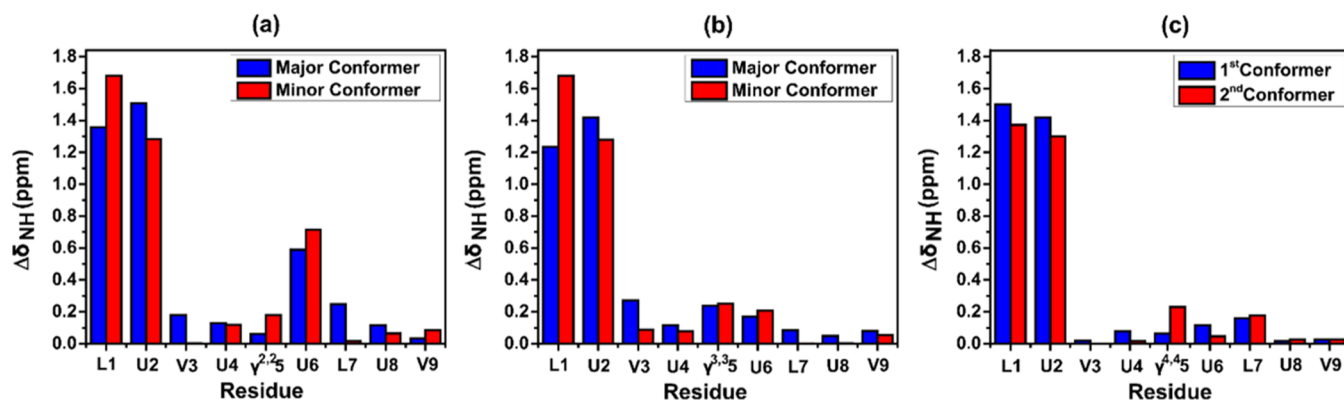


Figure 6. Plot of the change of the NH chemical shift value of the residues with increasing concentration of DMSO- d_6 (0–40%) in (a) P1, (b) P2, and (c) P3.

the DMSO- d_6 molecules in contrast to the terminal NH protons. In the case of the minor conformer of P1, Leu (1), Aib (2), and Aib (6) were nonhydrogen-bonded, suggesting a helical structure with six intramolecular hydrogen bonds. In P2, Leu (1) and Aib (2) NHs were completely solvent-exposed in both the conformers, while all of the other NHs seemed solvent-shielded. Earlier NOE studies suggested the ambidextrous helix and the right-handed CE $_{3,10}$ helix to be the major and minor conformers of P2 in solution. Leu (7) NH though nonhydrogen-bonded intramolecularly in the ambidextrous helical conformation observed in crystals (Figure S25) appeared as a hydrogen-bonded NH in the major conformer of P2 in the solvent titration experiment (Figure 6b) owing to the hydrogen bonding of Leu (7) NH to a water molecule. Though Val (3) NH was nonhydrogen-bonded in the CE $_{3,10}$ helical conformation observed in crystals due to the formation of the N-terminal three residue C $_{13}$ hydrogen bond (Figure 4c), it seemed hydrogen-bonded in the minor conformer of P2 from the titration experiment. This discrepancy might be due to the nonaccessibility of DMSO- d_6 molecules in the hydrophobic pocket of Val (3). In P3, Leu (1) and Aib (2) NHs were completely solvent-exposed or nonhydrogen-bonded in both the conformers, while all of the other NHs were solvent-shielded or hydrogen-bonded (Figure 6c). This observation corroborated exactly with the hydrogen bonding pattern observed in the CE $_{3,10}$ helices witnessed in the crystals (Figure 4d,e).

CD Spectroscopy. We have performed circular dichroism (CD) in acetonitrile on both the conformers present in the solution for P1–P3 (Figure 7). We separated the peaks via analytical HPLC, lyophilized them separately, and performed CD with each of the conformers. For the minor conformers of P1 and P2 and the later eluting conformer of P3, a prominent negative cotton effect peak was observed at around 206 nm and a minor peak was observed at around 225 nm, suggesting the presence of a right-handed helical conformation in them.^{42,43} For the major conformers of P1 and P2, positive cotton effect peaks were observed at 206 (for P1), 209 nm (for P2) (strong), and 220 nm (weak), respectively. Ambidextrous helices in DL peptides with left-handedness at the N-terminus were previously shown to manifest a positive cotton effect, while ambidextrous helices in LD peptides manifested a negative cotton effect.⁵ The observation of the positive cotton effect in the major conformers of P1 and P2 thus established ambidexterity with left-handedness at the N-terminus followed by right-handedness at the C-terminus, which was exactly in

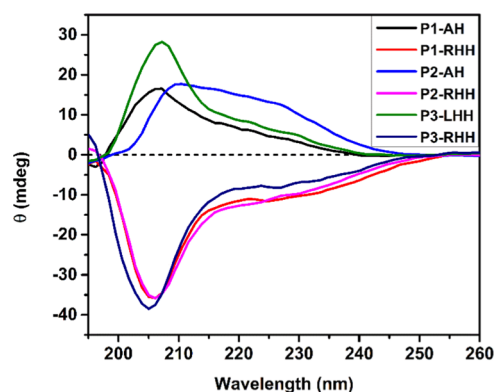


Figure 7. CD spectra of all of the conformers of P1–P3 in ACN at 600 μ M. All of the latter eluting conformers adopted a right-handed helical conformation in solution. The earlier eluting conformers adopted ambidextrous (for P1 and P2) and left-handed (for P3) helical conformations in solution, respectively. AH: Ambidextrous helix, LHH: left-handed helix, and RHH: right-handed helix.

line with our conclusions from the crystal structure and NMR data. A positive cotton effect was also observed for the early eluting conformer of P3, which was almost the mirror image of the negative cotton effect peak observed in the later eluting right-handed helical conformation of P3. This suggested a left-handed helical conformation in the earlier eluting peak. The greater intensity of the peak at 206 nm for the right-handed helical conformation in comparison to the left-handed helical conformation might be owing to the C-terminal fraying of the left-handed helix, as observed from the crystal structure. It should be noted that the right-handed helical conformations in the solution eluted later in comparison to the ambidextrous helical conformation or the left-handed helical conformation. This was in line with a report where LL dipeptides eluted later in comparison to the LD/DD dipeptides.⁴⁴ In summary, CD experiments established the presence of a major ambidextrous helical conformation and a minor right-handed helical conformation in solution for P1 and P2, while the coexistence of both left and right-handed helical conformations for the case of P3.

DFT-Optimized Structures and Energetics. In order to gain insights into the structure of the minor conformation of P1 (observed in solution but not in crystals) and to understand the energetic origin of the population distribution of the various conformations in solution, we performed DFT calculations (see SI). As no crystals were obtained for the

minor conformer of **P1**, the DFT calculations in this case were performed on a **P1** model having a right-handed CE₃₁₀ helical conformation (decided primarily considering the ROESY, solvent titration studies and the observation of a CE₃₁₀ right-handed helical conformation in the case of **P2** and **P3**). Figures 8 and S32 show the optimized structures of **P1**–**P3**. The

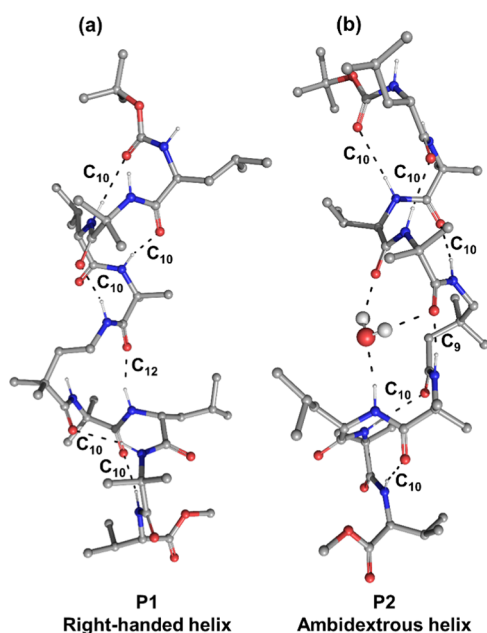


Figure 8. Optimized structures of (a) minor conformer of **P1** (right-handed CE₃₁₀ helix) and (b) major conformer of **P2** (ambidextrous helix) from DFT calculations.

torsion angle values and the hydrogen bond parameters in the optimized structures were in close agreement with the crystal structure parameters (Tables 1 and 2). All of the optimized structures were found to be true minima in the potential energy hypersurface (supported by all positive frequencies obtained from normal mode analysis). The optimized structure of the **P1** minor conformer (Figure 8a) was helical and stabilized by a series of six two-membered hydrogen bonds. There were three N-terminal C₁₀ hydrogen bonds, followed by one $\gamma\alpha$ C₁₂ hydrogen bond and two C-terminal C₁₀ hydrogen bonds. One of the C₁₂ hydrogen bonds across the Aib (4)- $\gamma^{2,2}$ (5) segment was absent, resulting in the solvent exposure of Aib (6) NH, which was seen earlier in the DMSO-*d*₆ titration experiments (Figure 6a). The $\gamma^{2,2}$ residue adopted a folded conformation about the disubstituted C ^{α} carbon atom ($\theta_2 = -62.1^\circ$, $\psi = -54.6^\circ$) and a (−+−−) combination of signs of the torsion angles. Right-handed CE₃₁₀ helices formed by the $\gamma^{3,3}$ and $\gamma^{4,4}$ amino acid residues (Figure 4c,e) were seen to form two C₁₂ hydrogen bonds each, unlike the $\gamma^{2,2}$ residue (Figure 8a). This might be an indication that the $\gamma^{2,2}$ residue was less prone to adopt a C₁₂ helical conformation in comparison to the $\gamma^{3,3}$ and $\gamma^{4,4}$ residues. The computed structure for the major conformer of **P2** (Figure 8b) had torsion angles and hydrogen bond parameters in good agreement (Table 2) with that obtained from the crystal structure (low-resolution structure, Figure S25). Placement of the hydrogen atoms of the cocrystallized water molecule in the computed structure enabled the observation of three intermolecular hydrogen bonds between **P2** [Leu (7) NH, Val (3) CO and Aib (4) CO] and the water molecule. These

three intermolecular hydrogen bonds seemed to have induced a reversal of helix handedness in **P2**, unlike two such hydrogen bonds in the case of **P1**.

Figure 9 shows the relative energies of all of the conformations of **P1**–**P3** realized in solution and crystals.

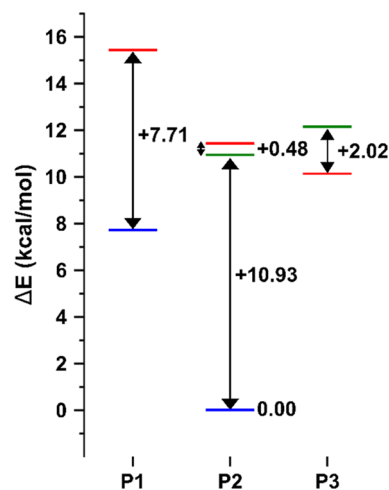


Figure 9. Relative energy diagram of the different conformations adopted by **P1**–**P3** in solid and solution states: Ambidextrous helices of **P1** and **P2** (blue line), right-handed CE₃₁₀ helix of **P1**–**P3** (red line), and left-handed CE₃₁₀ helix of **P2** and **P3** (green line). Ambidextrous helices of **P1** and **P2** are lower in energy and form major conformers in solution. Left- and right-handed CE₃₁₀ helices (enantiomeric except at the termini) have close energies and are equipopulated in the case of **P3**.

Several interesting observations were made from the energy calculations: (a) ambidextrous helices were the most stable conformers for **P1**/**P2** (which explained them being the major conformers in solution), (b) the ambidextrous helical conformation for **P2** was relatively more stable than that of **P1**, owing to one more water-mediated hydrogen bond in the former (Figures 4a and S25 and 8b), and (c) the energy difference between the major and minor conformers (~8, 11 and 2 kcal/mol for **P1**, **P2** and **P3** resp.) was proportional to their relative populations (60:40, 70:30 and 50:50 for **P1**, **P2** and **P3** resp.) in solution. The greater stability of the ambidextrous helices over the right-handed CE₃₁₀ helices of **P1** and **P2** might be owing to the greater number of hydrogen bonds in the former (7, 8 for **P1**, **P2**) with respect to the later (6, 6 for **P1**, **P2**) (Figures 4a–c and 8 and Table 2). A greater difference in the number of hydrogen bonds between the major and the minor conformers in the case of **P2** relative to **P1** led to a greater energy difference that consequently resulted in the higher population difference in **P2** (70:30) with respect to **P1** (60:40). High energy of the right-handed helical conformation of **P1** (minor conformer in solution) might have limited its realization in the crystal state. The left- and the right-handed helices of **P2** and **P3** have similar energies (0.5 and 2 kcal/mol), being almost enantiomeric (throughout the middle part of the helix with small differences at the termini) (Figure 4b–e). The small energy difference between the left and right-handed helical conformation in **P3** (Figure 9) led to similar populations of the two being observed in solution (Figures 1b and 2).

We performed DFT calculations with the single ambidextrous **P3** helix in the presence and absence of the key water

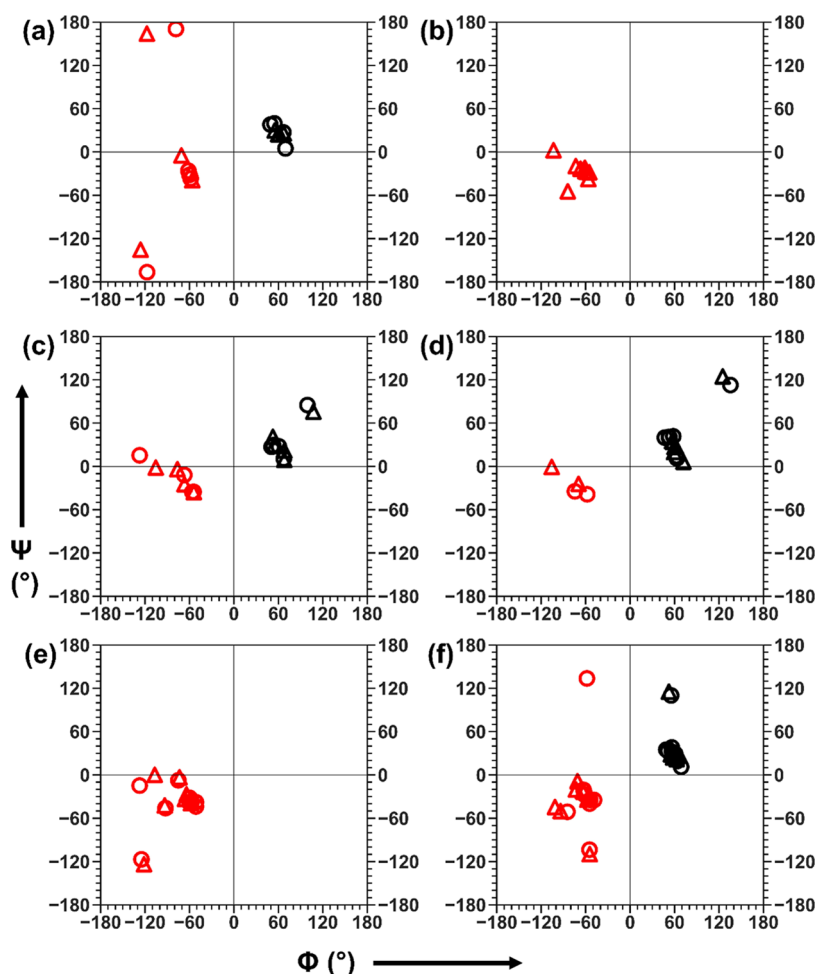


Figure 10. Ramachandran plot showing the ϕ and ψ values for the torsion angles of the α amino acid residues of the different conformations of **P1–P3** in the crystals and the DFT-computed structures. Red icons represent right-handedness, while black icons represent left-handedness. Open circles and triangles represent torsion angle values from crystal structures and DFT structures, respectively. Population distribution of the various conformations in solution is denoted in parentheses in each case. (a) **P1** ambidextrous helix (major conformer), (b) **P1** right-handed CE_{310} helix (minor conformer), (c) **P2** ambidextrous helix (major conformer), (d) **P2** left-handed CE_{310} helix, (e) **P2** right-handed (minor conformer), and (f) **P3** left- and right-handed CE_{310} helices (almost equipopulated conformers).

molecule (responsible for the reversal of handedness in the **P1** and **P2** ambidextrous helix). The results suggest that the ambidextrous **P3** is +14.3 kcal/mol (in the absence of the water molecule) and +4.6 kcal/mol (in the presence of the water molecule) higher in energy relative to the most stable **P2** ambidextrous isomer. (Figure S34) Thus, the **P3** ambidextrous helix including the key water molecule does not seem experimentally unrealizable from the energy point of view. However, it should be noted that a single **P3** molecule may not be an appropriate model for representing the self-assembly in a solution or solid state. Neighboring **P3** molecules might have a role in restricting water accessibility, thus disallowing the ambidextrous population of **P3** in solution or crystals.

Observation of Novel Conformations in P1–P3: A Discussion. The experimental and computational studies represented above established multiple distinct conformations adopted by **P1–P3**. **P1–P3** were composed of α amino acid residues of two types, the achiral Aib and the chiral L amino acid residues, Leu and Val, with a single centrally located achiral γ amino acid residue $\gamma^{x,x}$ ($x,x = 2,2/3,3/4,4$), thus making it overall chiral. As L amino acid residues are known to give rise to right-handed helical structures, **P1–P3** would have been expected to generate right-handed conformations as well.

However, in addition to the usually encountered right-handed CE_{310} helical conformation of the chiral L α amino acid-containing peptides, **P1–P3** adopted other striking and unprecedented conformations like:

1. Ambidextrous helical conformation (containing both right and left-handedness).
2. Left-handed CE_{310} helical conformation.

Figure 10 represents a conformational diagram that permits the understanding of the conformations of **P1–P3** with different handedness. Peptides **P1** and **P2** adopted the ambidextrous helical conformation. Though ambidextrous helices have been reported in $(\alpha\gamma^{3,3})_n$ hybrid peptides by Gopi and coworkers,⁷ they were achiral in nature. This, to the best of our knowledge, is the first report of the observation of ambidexterity in chiral peptides containing L amino acid residues. A closer look at the crystal structures revealed that the ambidextrous helical conformation was induced by the presence of a water molecule at the central part of the helix (close to the γ residue) in **P1** and **P2**. Both the peptides had right-handedness at the C-terminus and left-handedness at the N-terminus. The change in the handedness from right to left occurred at the Aib (4) residue (i.e. after the $\gamma^{2,2}$ residue) in

P1, while it occurred at the $\gamma^{3,3}$ residue for **P2**. A water molecule formed two hydrogen bonds with the Leu (7) NH and left-handed Aib (4) CO in **P1** and three hydrogen bonds with Leu (7) NH and left-handed Aib (4) CO and Val (3) CO in **P2**, respectively, inducing the change in handedness. This change in handedness obliterated the usual C_{12} hydrogen bonds across the Aib (4)– $\gamma^{x,x}$ (5) and $\gamma^{x,x}$ (5)–Aib (6) segments ($x = 2, 3$). To access the stabilizing effect of the water molecule in the ambidextrous conformers of **P1** and **P2**, the water molecule was removed, and the resulting structures were subjected to geometry optimization. Ambidexterity was preserved even without the water, but a significant energy penalty was evident from the estimated energetics. The energy difference ($\Delta E = E^{\text{ambidextrous}}(\text{without water}) + E^{\text{water}} - E^{\text{ambidextrous}}$) was calculated. Estimated energetics (ΔE) suggested that deleting the water destabilized the ambidextrous conformers by +10.6 and +10.74 kcal/mol for **P1** and **P2**, respectively. The destabilization was due to the loss of water-mediated hydrogen bonds (Figure S33). In a separate study on hexapeptides of this series, ambidextrous helices were seen to be stabilized by methanol-mediated H-bonds. Thus, water/solvent-mediated H-bond seems indispensable in the formation of the ambidextrous helical structure. The inability to accommodate a water molecule in the central region of **P3** (even in the presence of water in the crystallization solvent) might have led to the absence of the ambidextrous helix in this case. The position of disubstitution in the $\gamma^{4,4}$ amino acid residue might be responsible for this preferential inability in the recruitment of the water molecule in **P3**.

Achiral amino acid residues can adopt both left- and right-handed conformations with equal ease. The centrally located achiral γ amino acid residues $\gamma^{3,3}$ and $\gamma^{4,4}$ could thus adopt either right- or left-handedness and could induce this on its neighboring amino acid residues, irrespective of their chirality. However, this effect of induction of handedness on the neighboring residues (by the γ amino acid residue) seemed to be prominent only up to three amino acid residues, which resulted in the observation of diastereomers in the left- and right-handed helices of **P2** and **P3** (differing in stereochemistry at the 4th amino acid residues from γ).

In the left-handed $CE_{3,10}$ helices of **P2** and **P3**, the L amino acid residues [Val (3) and Leu (7)] in close proximity to the central achiral γ amino acid residues adopted left-handedness. However, residues Leu (1) and Val (9), which were further away from the central γ amino acid residue reverted back to their usual right-handed conformation in **P2** (Figure 4b and Table 1). In the case of **P3**, though Val (9) changed back to its usual right-handed conformation, the terminal Leu (1) still retained its left-handed conformation in the crystals. Thus, the observation of the left-handedness in **P2** and **P3** was a direct consequence of the centrally located achiral γ amino acid residue. No left-handed helices were experimentally realized either in a solution or a crystal for **P1**. Thus, similar abilities for $\gamma^{2,2}$ remain inconclusive.

CONCLUSIONS

Chiral peptides **P1–P3**, containing L amino acid residues, were established to be adopting a rare ambidextrous helical conformation and left-handed $CE_{3,10}$ helical conformation, in addition to the regular right-handed $CE_{3,10}$ helical conformation. Ambidexterity needing the reversal of handedness around the central part of the helix was induced by hydrogen bonds to a centrally positioned water molecule. The differential position

of disubstitution of the γ amino acid residue backbone in $\gamma^{4,4}$ of **P3** might have prevented the recruitment of water in the structure, thus preventing the formation of the ambidextrous helix in **P3**. The central achiral γ amino acid residues adopted either handedness and induced it on the flanking α amino acid residues irrespective of their configuration, thus generating left- and right-handed $CE_{3,10}$ helical conformations. This ability of induction of handedness of the central γ amino acid residues on the neighboring α amino acid residues (L or achiral) wore off with distance beyond three amino acid residues. The difference in stabilities between the different conformations of **P1–P3** determined their populations in solution. Among the three differentially disubstituted γ amino acid residues, $\gamma^{4,4}$ was most prone to adopting the $CE_{3,10}$ helical structure followed by $\gamma^{3,3}$. $\gamma^{2,2}$ seemed to be least prone to adopting the $CE_{3,10}$ helical structure among all three. The present study opens up different possibilities for the design of hybrid peptide architectures with mixed handedness through a rational design of peptides using appropriately disubstituted γ amino acid residues.

MATERIALS AND METHODS

All of the amino acids (except three unnatural γ amino acids⁴⁵) and coupling reagents 1-ethyl-3-(3-dimethylaminopropyl) carbodiimide hydrochloride (EDC-HCl) and 1-hydroxybenzotriazole (HOBt) were purchased from GL Biochem (Shanghai, China). Dioxane, trifluoroacetic acid (TFA), HPLC-graded acetonitrile, and methanol were obtained from Merck. Di-*tert*-butyl dicarbonate (Boc), thionyl chloride ($SOCl_2$), *N,N*-diisopropylethylamine (DIPEA), calcium hydride, lithium hydroxide (LiOH), and other chemicals were purchased from Sigma-Aldrich. Methanol and dichloromethane were dried using magnesium turnings and calcium hydride (CaH_2), respectively. All reagents for peptide synthesis were used as received without further purification. Column chromatography was done using silica gel (60–120 mesh size) as the stationary phase and hexane/ethyl acetate as an eluent. Thin-layer chromatography (TLC) was performed using TLC Silica Gel 60 F₂₅₄ and visualized by ultraviolet (UV) light or stained with iodine vapor and a $KMnO_4$ solution.

Peptide purification was done by reverse-phase high-performance liquid chromatography (RP-HPLC) using a Thermo Scientific Dionex Ultimate 3000 on a semipreparative Luna 5 μm C18(2) 100 Å, LC column (250 × 21.20 mm²). The purity of the peptides was confirmed using an Agilent 1260 Infinity II Prime LC analytical HPLC system with an Agilent Technologies ZORBAX Eclipse Plus C18 analytical column (5 μm , 4.6 × 250 mm²). Matrix-assisted laser desorption/ionization-time of flight (MALDI-TOF) was measured using a Bruker Daltonics Autoflex speed analysis instrument. Electrospray ionization-MS (ESI-MS) was measured using an Agilent-Q-TOF LC/MS 6500 instrument by electrospray ionization positive mode, equipped with Mass Hunter workstation software.

1D and 2D NMR spectra were recorded on Bruker Ascend TM Aeon 400 and 600 MHz spectrometers. All spectra were recorded in $CDCl_3$. The coupling constant (J) was measured in Hertz. The chemical shift values are reported in ppm downfield from tetramethylsilane, using $CDCl_3$ ($\delta = 7.26$ ppm for ¹H NMR).

General Procedure of Peptide Synthesis (P1–P3). All peptides (**P1–P3**) were synthesized through conventional solution-phase chemistry using a fragment condensation strategy involving a 3 + 6 coupling in the final step. *tert*-

Butyloxycarbonyl (Boc) was used for N-terminus protection, and the C-terminus was protected as a methyl ester. Peptide coupling was mediated by EDC-HCL and HOBt. Deprotection of the Boc group was achieved by TFA in DCM (1:1), and the methyl group was removed by saponification using LiOH in a mixture of methanol and water (2:1). (Scheme S1)

Purification. Crude peptides were purified by reverse-phase HPLC using a binary methanol/water (92–100%) solvent system at a flow rate of 10 mL/min using dual UV detection at 214 and 220 nm. To check the purity, analytical HPLC was performed with a flow rate of 1 mL/min and a linear gradient of 50–100% in an acetonitrile/water system. (Figure 1b).

Characterization of Peptides P1–P3. Boc–Leu–Aib–Val–Aib– γ^2 –Aib–Leu–Aib–Val–OMe (P1). ^1H NMR (600 MHz, chloroform-*d*) (Figure S5): δ 7.92 (d, $J = 6.3$ Hz), 7.72 (s), 7.58 (s), 7.53 (s), 7.38 (s), 7.33 (d, $J = 8.2$ Hz), 7.26 (br) 7.24–7.20 (br), 7.19 (s), 7.12 (d, $J = 6.0$ Hz), 7.06 (s), 6.96 (s), 6.77 (s), 6.67 (s), 5.16 (s), 5.11 (s), 4.43–4.39 (m), 4.27 (ddd, $J = 10.4, 6.5, 2.8$ Hz), 4.00–3.95 (m), 3.90 (t, $J = 5.9$ Hz), 3.87–3.81 (m), 3.78 (t, $J = 6.1$ Hz), 3.70–3.69 (br), 3.28–3.22 (m), 3.21–3.13 (m), 3.08–2.97 (m), 2.22 (dh, $J = 19.4, 6.7$ Hz), 1.86–1.71 (m), 1.66–1.57 (m), 1.56–1.43 (m), 1.17 (br, $J = 8.8$ Hz), 1.11 (br), 1.01–0.90 (m). $^{13}\text{C}\{^1\text{H}\}$ NMR (150 MHz, chloroform-*d*) (Figure S8): δ 177.9, 175.6, 175.5, 175.3, 172.6, 172.5, 172.0, 170.7, 156.3 (d, $J = 86.7$ Hz), 80.9, 65.8, 61.7, 61.6, 58.2, 57.9, 57.3, 57.2, 56.9, 56.8, 56.7, 56.7, 55.3, 53.8, 53.4, 53.1, 51.8, 51.7, 42.0, 41.7, 40.2, 40.1, 39.6, 39.4, 38.9, 38.6, 37.0, 36.9, 30.7, 30.6, 29.3, 29.1, 28.3, 28.2, 27.7, 27.6, 27.3, 27.2, 27.1, 27.1, 26.4, 26.1, 25.9, 25.4, 25.2, 25.0, 24.9, 24.9, 24.9, 24.8, 24.8, 24.6, 23.9, 23.5, 23.4, 23.4, 23.3, 23.2, 23.0, 22.7, 21.8, 21.7, 21.1, 21.0, 19.3, 19.1, 19.1, 19.1, 18.7, 18.4, 18.3, 18.2. MALDI-TOF of P1, analytical HPLC peak at (a) 9.7 min [calc. (M + Na + 2H) $^+$ for $\text{C}_{50}\text{H}_{91}\text{N}_9\text{O}_{12} = 1034.6841$ Da obs. = 1034.093 Da] and (b) 10.3 min [calc. (M + K) $^+$ for $\text{C}_{50}\text{H}_{91}\text{N}_9\text{O}_{12} = 1048.6424$ Da obs. = 1049.186 Da] (Figure S2).

Boc–Leu–Aib–Val–Aib– γ^3 –Aib–Leu–Aib–Val–OMe (P2). ^1H NMR (600 MHz, chloroform-*d*) (Figure S6): δ 8.36 (d, $J = 5.0$ Hz), 8.17 (s), 7.86–7.78 (br), 7.75 (s), 7.67 (s), 7.58 (s), 7.51 (s), 7.44 (d, $J = 8.8$ Hz), 7.42 (d, $J = 8.8$), 7.00 (d, $J = 6.5$), 6.96 (s), 6.86 (d, $J = 10.4$ Hz), 6.77 (d, $J = 8.4$ Hz), 6.70 (s), 6.65 (s), 5.20 (s), 5.11 (s), 4.41 (dt, $J = 8.1, 6.0$ Hz), 4.18 (q, $J = 6.4$ Hz), 4.03–3.96 (m), 3.88 (t, $J = 6.0$ Hz), 3.86–3.81 (m), 3.75–3.71 (br), 3.71 (s), 3.68 (s), 3.54 (t, $J = 11.6$ Hz), 2.74 (d, $J = 13.7$ Hz), 2.54 (d, $J = 13.7$), 2.34–2.29 (m), 2.27–2.19 (m), 1.96 (d, $J = 13.7$ Hz), 1.94–1.87 (m), 1.86–1.77 (m), 1.75–1.62 (m), 1.58 (s), 1.57–1.43 (m), 1.20 (s), 1.13 (br), 1.02–0.91 (m). $^{13}\text{C}\{^1\text{H}\}$ NMR (150 MHz, chloroform-*d*) (Figure S9): δ 175.6, 175.3, 174.8, 172.5, 172.5, 172.2, 171.8, 171.3, 156.3 (d, $J = 95.9$ Hz), 81.0, 65.8, 61.2, 58.3, 58.0, 57.4, 57.2, 57.0, 56.9, 56.8, 56.7, 56.6, 54.1, 53.8, 53.4, 51.8, 51.6, 48.3, 43.6, 40.3, 39.3, 38.2, 35.2, 30.6, 30.6, 29.7, 29.2, 28.3, 28.2, 27.9, 27.8, 27.7, 27.5, 27.3, 27.2, 26.7, 26.6, 26.6, 25.4, 25.0, 24.9, 24.8, 24.6, 24.2, 23.6, 23.5, 23.2, 23.2, 23.0, 22.9, 22.6, 21.9, 21.7, 21.0, 20.8, 19.3, 19.2, 19.1, 18.4, 18.3, 18.2, 17.9, 15.2. MALDI-TOF of P2, analytical HPLC peak at (a) 11.3 min [calc. (M + Na + H) $^+$ for $\text{C}_{50}\text{H}_{91}\text{N}_9\text{O}_{12} = 1033.6763$ Da Obs. = 1033.411 Da] and (b) 12.7 min [Calc. (M + Na + H) $^+$ for $\text{C}_{50}\text{H}_{91}\text{N}_9\text{O}_{12} = 1033.6763$ Da obs. = 1033.299 Da] (Figure S3).

Boc–Leu–Aib–Val–Aib– γ^4 –Aib–Leu–Aib–Val–OMe (P3). ^1H NMR (600 MHz, Chloroform-*d*) (Figure S7): δ 8.18

(s), 8.02 (s), 7.58 (s), 7.55 (s), 7.54–7.51 (br), 7.46 (d, $J = 6.7$ Hz), 7.39 (s), 7.29 (d, $J = 8.4$ Hz), 7.25 (d, $J = 8.3$), 7.12 (d, $J = 5.4$ Hz), 6.79 (s), 6.72 (s), 6.58 (s), 6.48 (s), 5.39 (s), 5.22 (s), 4.41 (ddd, $J = 8.2, 6.2, 3.5$ Hz), 4.25–4.19 (m), 4.12 (ddd, $J = 11.2, 7.1, 4.4$ Hz), 3.90–3.83 (m), 3.82–3.76 (m), 3.71 (s), 3.69 (s), 2.70–2.62 (m), 2.48 (dd, $J = 15.5, 7.3$ Hz), 2.28–2.16 (m), 1.90–1.77 (m), 1.69–1.60 (m), 1.59–1.56 (m), 1.54–1.48 (m), 1.48–1.43 (m), 1.33 (s), 1.31 (s), 1.20 (s), 1.16 (s), 1.03–0.95 (m), 0.93–0.89 (m). $^{13}\text{C}\{^1\text{H}\}$ NMR (150 MHz, Chloroform-*d*) (Figure S10): δ 175.8, 175.6, 175.5, 172.6, 172.5, 172.0, 156.1, 80.8, 65.8, 61.9, 61.7, 58.2, 58.1, 57.3, 57.2, 57.1, 57.0, 56.9, 56.6, 56.5, 56.4, 55.5, 53.8, 53.7, 53.6, 53.2, 51.8, 51.7, 40.3, 39.4, 38.6, 34.7, 34.6, 31.0, 30.7, 30.7, 30.2, 29.6, 29.2, 28.3, 28.2, 27.9, 27.8, 27.6, 27.4, 27.4, 27.3, 27.2, 27.0, 26.8, 26.7, 25.6, 25.3, 25.0, 24.9, 24.8, 24.6, 24.6, 23.5, 23.5, 23.4, 23.4, 23.3, 23.2, 23.0, 22.6, 22.5, 21.9, 21.6, 21.1, 20.8, 19.3, 19.2, 19.1, 19.0, 18.8, 18.3, 18.3, 15.2. MALDI-TOF of P3, analytical HPLC peak at (a) 10.9 min [calc. (M + Na + H) $^+$ for $\text{C}_{50}\text{H}_{91}\text{N}_9\text{O}_{12} = 1033.6763$ Da obs. = 1033.171 Da] and (b) 12.4 min [calc. (M + Na + H) $^+$ for $\text{C}_{50}\text{H}_{91}\text{N}_9\text{O}_{12} = 1033.6763$ Da obs. = 1033.145 Da.] (Figure S4).

Single-Crystal X-ray Diffraction. Crystallization of all of the peptide conformers was carried out primarily in an acetonitrile/H₂O system either from mixtures of conformations or HPLC-separated fractions. For P1, crystals were grown from a mixture of conformers in an ACN/H₂O solvent system. Crystals could not be grown from the isolated minor peak. More than one crystals could be grown for P2 and P3. In the case of P2, distinct crystals could be grown from the mixture of conformations in ACN/H₂O and ACN/MeOH/H₂O solvent systems. The third crystal for P2 was grown from the separated minor conformer fraction from the ACN/H₂O solvent system. In the case of P3, distinct crystals were grown from the mixture of conformers and from the isolated fraction (the later eluting peak in the HPLC chromatogram) in the ACN/H₂O solvent system. Data were collected at temperatures of 105, 176, and 297 K, respectively. One of the crystal structures of P2 (grown from a mixture in ACN/H₂O) could not be refined well. Tables S9 and S10 provide the crystal and refinement parameters for all of the peptide structures. Intensity data were collected with Mo-K α radiation ($\lambda = 0.71073$ Å) by a Bruker (D8 Quest) diffractometer. Data were processed using the Bruker SAINT package. All of the structures were solved by direct methods using either SHELXS (right-handed helix of P3) or SHELXD (all except right-handed helix of P3)^{46,47} and were refined using the least-squares method in SHELXL-14.⁴⁸ All hydrogen atoms were fixed in ideal geometries and were refined as riding against the atoms to which they are bonded. The crystal structures have been deposited at the Cambridge Crystallographic Data Centre (CCDC) with deposition numbers 2206582–2206586.

FTIR Spectroscopy. Solution IR spectroscopy of all peptides was carried out by using a PerkinElmer Spectrum Two spectrometer. All FTIR spectra were recorded in the region of 400–4000 cm⁻¹. For this study, peptides were dissolved in CDCl₃ at 1 mM concentrations, and before casting the sample, the solvent as a sample was recorded to prevent the appearance of solvent peaks in the spectrum.

NMR Spectroscopy. All NMR experiments were carried out on a Bruker Ascend Aeon 600 and 400 MHz spectrometer, respectively. The peptide concentrations were in the range of

5–7 mM in CDCl₃ for both 1D and 2D NMR experiments. The chemical shift values and coupling constants were measured from 1D NMR spectra. Variable temperature 1D NMR experiments were carried out between 273 and 323 K. Complete resonance assignments of the protons of P1–P3 were done by TOCSY and ROESY experiments. All of the 2D experiments were done in phase-sensitive mode by using the time-proportional phase incrementation (TPPI) method. For all peptides, TOCSY spectra were recorded with a mixing time of 80 ms, but for ROESY spectra, three different mixing times of 150 (for P1), 250 (for P2), and 300 ms (for P3) were used, respectively. The spectral width was 6009.6 Hz in both dimensions. The total number of scans was fixed to 32 for TOCSY and ROESY, respectively. Data points were set to 2048 and 300 in f2 and f1 dimensions, respectively, for both TOCSY and ROESY spectra. Zero filling was done to finally yield a data set of 4K × 2K. All NMR spectra were processed using Topspin 3.6 software.

CD Spectroscopy. The CD spectra of all of the solution conformers of P1–P3 were recorded by using a 200 μL quartz cuvette of a 1 mm path length with a Jasco J-1500 spectropolarimeter at room temperature. The CD studies were performed in acetonitrile at 600 μM concentrations for all peptides. Spectra were collected at a scan rate of 100 nm·min⁻¹ and 2 nm bandwidth from 190 to 260 nm with five scans for averaging. Before running the sample, acetonitrile was run to correct the baseline.

Electronic Structure Calculations. 2D NMR experiments confirmed that the peptides (P1, P2, and P3) are helical and have two distinct conformations. DMSO-*d*₆ titration experiments also highlighted the backbone NHs that are solvent-exposed. However, the structure of the one conformer could not be crystallized. To gain insights into the structures, we performed computational modeling. Using the experimental data as an input, we modeled helical peptides in PyMOL software⁴⁹ and subjected these models to geometry optimization using the Gaussian 16 program⁵⁰ employing density functional theory (B3LYP/6-311++G* level).^{51–53} Calculations also included normal mode frequency calculations to identify the nature of the structures in the energy hypersurface. The optimized coordinates of the two conformers of peptides (P1, P2, and P3) are provided at the end of this document.

Relative Energies of Different Conformers Shown in Figure 9. The energy difference between two different optimized conformers (Δ*E*) was calculated with respect to the stable conformer. Thus, the estimated Δ*E* was always > 0.

- A. If two conformers did not contain a water molecule, then the relative energy between the two conformers was calculated using the equation

$$\Delta E = E^{C2}(Px) - E^{C1}(Px)$$

where Px = (P1 or P2 or P3) and C1/C2 = conformer1/2. The above equation was used to calculate +0.48 and +2.02 in Figure 9.

- B. If a water molecule was present in one of the conformations, then the energy of water was subtracted. E.g., the energy difference between two conformers C1 = ambidextrous helix and C2 = right-handed CE₃₁₀ helix of P1 was estimated from

$$\Delta E = [E^{\text{right-handed CE}_{310} \text{ helix}}(\mathbf{P1}) + E(\text{water})] - E^{\text{ambidextrous helix}}(\mathbf{P1})$$

Thus, +7.71 and +10.93 were calculated from the above equation.

- C. The most stable conformer was the P2 ambidextrous helix. Thus, all of the other energy levels were placed with respect to the P2 ambidextrous helix (0.0 of Figure 9).

■ ASSOCIATED CONTENT

Supporting Information

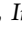
The Supporting Information is available free of charge at <https://pubs.acs.org/doi/10.1021/acsomega.3c05124>.

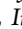
Reaction scheme, chemical structures, characterization spectra (¹H NMR, ¹³C NMR, MALDI-TOF), ESI-MS, analytical HPLC traces, TOCSY, temperature dependence of NH resonances, major conformer of P2 in the crystal, solution FTIR spectra, CSI plot, ROESY spectra, DMSO-*d*₆ titration plots, DFT structures, HPLC retention times, ¹H NMR parameters (chemical shifts, ³J_{NH–C^αH} values, Δ*δ* from DMSO-*d*₆ titration), crystallographic parameters, and Cartesian coordinates of DFT-calculated structures (PDF)

■ AUTHOR INFORMATION

Corresponding Authors

Prema G. Vasudev – Plant Biotechnology Division, CSIR-Central Institute of Medicinal and Aromatic Plants, Lucknow, Uttar Pradesh 226015, India; Email: premavasudev@cimap.res.in

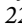
Priyadarshi Satpati – Biosciences and Bioengineering, Indian Institute of Technology, Guwahati, Guwahati, Assam 781039, India;  orcid.org/0000-0002-0391-3580; Email: psatpati@iitg.ac.in

Sunanda Chatterjee – Department of Chemistry, Indian Institute of Technology, Guwahati, Guwahati, Assam 781039, India;  orcid.org/0000-0001-5068-7208; Email: sunanda.c@iitg.ac.in

Authors

Swapna Debnath – Department of Chemistry, Indian Institute of Technology, Guwahati, Guwahati, Assam 781039, India

Vignesh Shanmugam Rajalakshmi – Biosciences and Bioengineering, Indian Institute of Technology, Guwahati, Guwahati, Assam 781039, India

Dinesh Kumar – Plant Biotechnology Division, CSIR-Central Institute of Medicinal and Aromatic Plants, Lucknow, Uttar Pradesh 226015, India;  orcid.org/0000-0003-2460-2551

Babulal Das – Department of Chemistry, Indian Institute of Technology, Guwahati, Guwahati, Assam 781039, India

Complete contact information is available at:

<https://pubs.acs.org/doi/10.1021/acsomega.3c05124>

Author Contributions

This manuscript was written through the contributions of all authors. All authors have given approval to the final version of the manuscript.

Notes

The authors declare no competing financial interest.

■ ACKNOWLEDGMENTS

SC acknowledges the Department of Science and Technology, India (Fast Track Project No: SB/FT/CS-070/2014) and the

Council for Scientific and Industrial Research, CSIR (01/ (2984)/19/EMR-II), for financial support. P.S. acknowledges SERB, Govt. of India (YSS/2015/000024) for funding. S.D. and V.S.R. acknowledge IIT Guwahati for the scholarship. COE-FAST(MHRD) is acknowledged for the 400 MHz NMR spectrometer, and the DST-FIST program 2017 (Sanction no. SR/ST/CS-II/2017/23C) is acknowledged for the X-ray diffractometer. Central Instruments Facility, IITG, is acknowledged for the NMR instrument facility. PARAM-ISHAN, Biomolecular Simulation Lab (BSL) of Department of Biosciences and Bioengineering and BIF facility (Supported by DBT, Project Code: BT/BI/12/064/2012) (NER-BIF) of IIT Guwahati is gratefully acknowledged for providing the computing facility. D.K. and P.G.V. acknowledge the Director, CSIR-CIMAP, for the infrastructure facilities. D.K. acknowledges Senior Research Fellowship from CSIR, India.

REFERENCES

- (1) Novotny, M.; Kleywegt, G. J. A survey of left-handed helices in protein structures. *J. Mol. Biol.* **2005**, *347*, 231–241.
- (2) Jourdan, F.; Lazzaroni, S.; Méndez, B. L.; Lo Cantore, P.; de Julio, M.; Amodeo, P.; Iacobellis, N. S.; Evidente, A.; Motta, A. A left-handed α -helix containing both L- and D-amino acids: The solution structure of the antimicrobial lipodepsipeptide tolaasin. *Proteins: Struct., Funct., Bioinf.* **2003**, *52*, 534–543.
- (3) Choi, S. H.; Guzei, I. A.; Spencer, L. C.; Gellman, S. H. Crystallographic characterization of 12-helical secondary structure in β -peptides containing side chain groups. *J. Am. Chem. Soc.* **2010**, *132*, 13879–13885.
- (4) She, F.; Teng, P.; Peguero-Tejada, A.; Wang, M.; Ma, N.; Odom, T.; Zhou, M.; Gjonaj, E.; Wojtas, L.; van der Vaart, A.; Cai, J. De Novo Left-Handed Synthetic Peptidomimetic Foldamers. *Angew. Chem., Int. Ed.* **2018**, *57*, 9916–9920.
- (5) Banerjee, A.; Raghobama, S. R.; Karle, I. L.; Balam, P. Ambidextrous molecules: Cylindrical peptide structures formed by fusing left- and right-handed helices. *Biopolymers* **1996**, *39*, 279–285.
- (6) Sudha, R.; Jarrold, M. F. Left-handed and ambidextrous helices in the gas phase. *J. Phys. Chem. B* **2005**, *109*, 11777–11780.
- (7) Misra, R.; George, G.; Saseendran, A.; Raghobama, S.; Gopi, H. N. Ambidextrous α , γ -Hybrid Peptide Foldamers. *Chem. - Asian J.* **2019**, *14*, 4408–4414.
- (8) Burkhart, B. M.; Gassman, R. M.; Langs, D. A.; Pangborn, W. A.; Duax, W. L. Heterodimer formation and crystal nucleation of gramicidin D. *Biophys. J.* **1998**, *75*, 2135–2146.
- (9) Bunkóczi, G.; Vértsey, L.; Sheldrick, G. M. The antiviral antibiotic feglymycin: first direct-methods solution of a 1000+ equal-atom structure. *Angew. Chem., Int. Ed.* **2005**, *44*, 1340–1342.
- (10) Aravinda, S.; Shamala, N.; Balam, P. Aib residues in peptaibiotics and synthetic sequences: analysis of nonhelical conformations. *Chem. Biodiversity* **2008**, *5*, 1238–1262.
- (11) Venkatraman, J.; Shankaramma, S. C.; Balam, P. Design of folded peptides. *Chem. Rev.* **2001**, *101*, 3131–3152.
- (12) Karle, I. L.; Balam, P. Structural characteristics of α -helical peptide molecules containing Aib residues. *Biochemistry* **1990**, *29*, 6747–6756.
- (13) Toniolo, C.; Crisma, M.; Formaggio, F.; Peggion, C. Control of peptide conformation by the Thorpe-Ingold effect (*Ca*-tetrasubstitution). *Biopolymers* **2001**, *60*, 396–419.
- (14) Le Bailly, B. A. F.; Clayden, J. Dynamic foldamer chemistry. *Chem. Commun.* **2016**, *52*, 4852–4863.
- (15) Crisma, M.; De Zotti, M.; Formaggio, F.; Peggion, C.; Moretto, A.; Toniolo, C. Handedness preference and switching of peptide helices. Part II: Helices based on noncoded α -amino acids. *J. Pept. Sci.* **2015**, *21*, 148–177.
- (16) Clayden, J.; Castellanos, A.; Solà, J.; Morris, G. A. Quantifying end-to-end conformational communication of chirality through an achiral peptide chain. *Angew. Chem., Int. Ed.* **2009**, *48*, 5962–5965.
- (17) Solà, J.; Morris, G. A.; Clayden, J. Measuring screw-sense preference in a helical oligomer by comparison of ^{13}C NMR signal separation at slow and fast exchange. *J. Am. Chem. Soc.* **2011**, *133*, 3712–3715.
- (18) Solà, J.; Helliwell, M.; Clayden, J. Interruption of a 310-helix by a single Gly residue in a poly-Aib motif: A crystallographic study. *Biopolymers* **2011**, *95*, 62–69.
- (19) Brown, R. A.; Marcelli, T.; De Poli, M.; Solà, J.; Clayden, J. Induction of unexpected left-handed helicity by an N-terminal L-amino acid in an otherwise achiral peptide chain. *Angew. Chem., Int. Ed.* **2012**, *51*, 1395–1399.
- (20) Boddaert, T.; Solà, J.; Helliwell, M.; Clayden, J. Chemical communication: conductors and insulators of screw-sense preference between helical oligo (aminoisobutyric acid) domains. *Chem. Commun.* **2012**, *48*, 3397–3399.
- (21) Solà, J.; Helliwell, M.; Clayden, J. N-versus C-terminal control over the screw-sense preference of the configurationally achiral, conformationally helical peptide motif Aib8GlyAib8. *J. Am. Chem. Soc.* **2010**, *132*, 4548–4549.
- (22) Abele, S.; Seiler, P.; Seebach, D. Synthesis, Crystal Structures, and Modelling of β -Oligopeptides Consisting of 1-(Aminomethyl) cyclopropanecarboxylic Acid: Ribbon-Type Arrangement of Eight-Membered H-Bonded Rings. *Helv. Chim. Acta* **1999**, *82*, 1559–1571.
- (23) Vasudev, P. G.; Shamala, N.; Ananda, K.; Balam, P. C9 Helices and ribbons in γ -peptides: crystal structures of gabapentin oligomers. *Angew. Chem., Int. Ed.* **2005**, *44*, 4972–4975.
- (24) Chatterjee, S.; Vasudev, P. G.; Raghobama, S.; Ramakrishnan, C.; Shamala, N.; Balam, P. Expanding the peptide β -turn in $\alpha\gamma$ hybrid sequences: 12 atom hydrogen bonded helical and hairpin turns. *J. Am. Chem. Soc.* **2009**, *131*, 5956–5965.
- (25) Misra, R.; Saseendran, A.; George, G.; Veeresh, K.; Raja, K. M. P.; Raghobama, S.; Hofmann, H. J.; Gopi, H. N. Structural Dimorphism of Achiral α , γ -Hybrid Peptide Foldamers: Coexistence of 12- and 15/17-Helices. *Chem. - Eur. J.* **2017**, *23*, 3764–3772.
- (26) Seebach, D.; Beck, A. K.; Bierbaum, D. J. The world of β - and γ -peptides comprised of homologated proteinogenic amino acids and other components. *Chem. Biodiversity* **2004**, *1*, 1111–1239.
- (27) Horne, W. S.; Gellman, S. H. Foldamers with heterogeneous backbones. *Acc. Chem. Res.* **2008**, *41*, 1399–1408.
- (28) Cheng, R. P.; Gellman, S. H.; DeGrado, W. F. β -Peptides: from structure to function. *Chem. Rev.* **2001**, *101*, 3219–3232.
- (29) Fülöp, F.; Martinek, T. A.; Tóth, G. K. Application of alicyclic β -amino acids in peptide chemistry. *Chem. Soc. Rev.* **2006**, *35*, 323–334.
- (30) Guichard, G.; Huc, I. Synthetic foldamers. *Chem. Commun.* **2011**, *47*, 5933–5941.
- (31) Vasudev, P. G.; Chatterjee, S.; Shamala, N.; Balam, P. Structural chemistry of peptides containing backbone expanded amino acid residues: conformational features of β , γ , and hybrid peptides. *Chem. Rev.* **2011**, *111*, 657–687.
- (32) Martinek, T. A.; Fülöp, F. Peptidic foldamers: ramping up diversity. *Chem. Soc. Rev.* **2012**, *41*, 687–702.
- (33) Bouillere, F.; Thétiot-Laurent, S.; Kouklovsky, C.; Alezra, V. Foldamers containing γ -amino acid residues or their analogues: structural features and applications. *Amino Acids* **2011**, *41*, 687–707.
- (34) Shin, S.; Lee, M.; Guzei, I. A.; Kang, Y. K.; Choi, S. H. 12/10-helical β -peptide with dynamic folding propensity: coexistence of right- and left-handed helices in an enantiomeric foldamer. *J. Am. Chem. Soc.* **2016**, *138*, 13390–13395.
- (35) Basuroy, K.; Dinesh, B.; Reddy, M. M.; Chandrappa, S.; Raghobama, S.; Shamala, N.; Balam, P. Unconstrained homooligomeric γ -peptides show high propensity for C14 helix formation. *Org. Lett.* **2013**, *15*, 4866–4869.
- (36) Gasparro, F. P.; Kolodny, N. H. NMR determination of the rotational barrier in N, N-dimethylacetamide. A physical chemistry experiment. *J. Chem. Educ.* **1977**, *54*, 258–261.
- (37) Vasudev, P. G.; Chatterjee, S.; Ananda, K.; Shamala, N.; Balam, P. Hybrid $\alpha\gamma$ Polypeptides: Structural Characterization of a

- C12/C10 Helix with Alternating Hydrogen-Bond Polarity. *Angew. Chem.* **2008**, *120*, 6530–6532.
- (38) Krimm, S.; Bandekar, J. Vibrational spectroscopy and conformation of peptides, polypeptides, and proteins. *Adv. Protein Chem.* **1986**, *38*, 181–364.
- (39) Jackson, M.; Mantsch, H. H. The use and misuse of FTIR spectroscopy in the determination of protein structure. *Crit. Rev. Biochem. Mol. Biol.* **1995**, *30*, 95–120.
- (40) Ulrich, E. L.; Akutsu, H.; Dorelejers, J. F.; Harano, Y.; Ioannidis, Y. E.; Lin, J.; Livny, M.; Mading, S.; Maziuk, D.; Miller, Z.; et al. BioMagResBank. *Nucleic Acids Res.* **2007**, *36*, 402–408.
- (41) Wishart, D. S.; Sykes, B. D.; Richards, F. M. The chemical shift index: a fast and simple method for the assignment of protein secondary structure through NMR spectroscopy. *Biochemistry* **1992**, *31*, 1647–1651.
- (42) Toniolo, C.; Formaggio, F.; Woody, R. W. *Comprehensive Chiroptical Spectroscopy*; Berova, N.; Polavarapu, P. L.; Nakanishi, K.; Woody, R. W., Eds.; John Wiley & Sons: Hoboken, NJ, 2012; Vol. 2, pp 499–544.
- (43) Karle, I. L.; Flippen-Anderson, J. L.; Sukumar, M.; Uma, K.; Balaram, P. Modular design of synthetic protein mimics. Crystal structure of two seven-residue helical peptide segments linked by epsilon-aminocaproic acid. *J. Am. Chem. Soc.* **1991**, *113*, 3952–3956.
- (44) Zbrozek, J.; Pumera, M.; Flegel, M. Chiral analysis of biogenic D, L-amino acids derivatized by N-fluorenylmethoxycarbonyl-L-alanyl N-carboxyanhydride using high-performance liquid chromatography. *J. Chromatogr. Sci.* **2002**, *40*, 505–508.
- (45) Debnath, S.; Ghosh, S.; Pandit, G.; Satpati, P.; Chatterjee, S. Effect of Differential Geminal Substitution of γ Amino Acid Residues at the (i+ 2) Position of $\alpha\gamma$ Turn Segments on the Conformation of Template β -Hairpin Peptides. *J. Org. Chem.* **2021**, *86*, 11310–11323.
- (46) Sheldrick, G. M. A short history of SHELX. *Acta Crystallogr., Sect. A: Found. Crystallogr.* **2008**, *64*, 112–122.
- (47) Schneider, T. R.; Sheldrick, G. M. Substructure solution with SHELXD. *Acta Crystallogr., Sect. D: Biol. Crystallogr.* **2002**, *58*, 1772–1779.
- (48) Sheldrick, G. M. Crystal structure refinement with SHELXL. *Acta Crystallogr., Sect. C: Struct. Chem.* **2015**, *71*, 3–8.
- (49) *The PyMOL Molecular Graphics System*, Version 2.0; Schrödinger, LLC.
- (50) Frisch, M. J.; Trucks, G. W.; Schlegel, H. B.; Scuseria, G. E.; Robb, M. A.; Cheeseman, J. R.; Scalmani, G.; Barone, V.; Petersson, G. A.; Nakatsuji, H.; Li, X.; Caricato, M.; Marenich, A. V.; Bloino, J.; Janesko, B. G.; Gomperts, R.; Mennucci, B.; Hratchian, H. P.; Ortiz, J. V.; Izmaylov, A. F.; Sonnenberg, J. L.; Williams-Young, D.; Ding, F.; Lipparini, F.; Egidi, F.; Goings, J.; Peng, B.; Petrone, A.; Henderson, T.; Ranasinghe, D.; Zakrzewski, V. G.; Gao, J.; Rega, N.; Zheng, G.; Liang, W.; Hada, M.; Ehara, M.; Toyota, K.; Fukuda, R.; Hasegawa, J.; Ishida, M.; Nakajima, T.; Honda, Y.; Kitao, O.; Nakai, H.; Vreven, T.; Throssell, K.; Montgomery, J. A., Jr; Peralta, J. E.; Ogliaro, F.; Bearpark, M. J.; Heyd, J. J.; Brothers, E. N.; Kudin, K. N.; Staroverov, V. N.; Keith, T. A.; Kobayashi, R.; Normand, J.; Raghavachari, K.; Rendell, A. P.; Burant, J. C.; Iyengar, S. S.; Tomasi, J.; Cossi, M.; Millam, J. M.; Klene, M.; Adamo, C.; Cammi, R.; Ochterski, J. W.; Martin, R. L.; Morokuma, K.; Farkas, O.; Foresman, J. B.; Fox, D. J. *Gaussian 16, Revision C.01*; Gaussian, Inc.: Wallingford CT, 2016.
- (51) Becke, A. D. Density-functional exchange-energy approximation with correct asymptotic behavior. *Phys. Rev. A* **1988**, *38*, 3098–3100.
- (52) Lee, C.; Yang, W.; Parr, R. G. Development of the Colle-Salvetti correlation-energy formula into a functional of the electron density. *Phys. Rev. B* **1988**, *37*, 785–789.
- (53) Jensen, F. Atomic orbital basis sets. *Wiley Interdiscip. Rev.: Comput. Mol. Sci.* **2013**, *3*, 273–295.